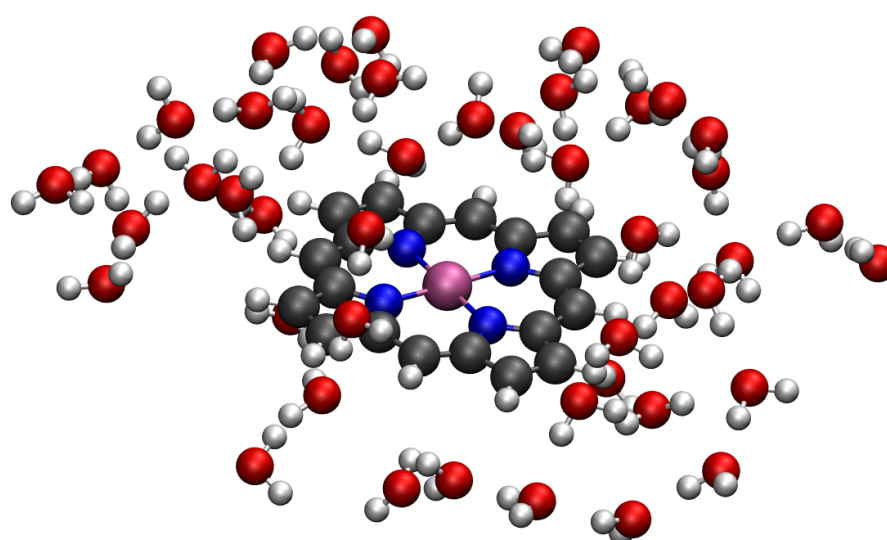


# CHALMERS



## Water Oxidation on Porphyrines

A First-principles Study

ADAM ARVIDSSON

Department of Applied Physics

*Division of Chemical Physics*

CHALMERS UNIVERSITY OF TECHNOLOGY

Gothenburg, Sweden 2014



Thesis for the degree of Master of Science in Engineering Physics

# Water Oxidation on Porphyrines

A First-principles Study

ADAM ARVIDSSON



Department of Applied Physics  
*Division of Chemical Physics*  
CHALMERS UNIVERSITY OF TECHNOLOGY  
Gothenburg, Sweden 2014

Water Oxidation on Porphyrines  
A First-principles Study  
ADAM ARVIDSSON

© ADAM ARVIDSSON, 2014

Department of Applied Physics  
Division of Chemical Physics  
Chalmers University of Technology  
SE-412 96 Gothenburg  
Sweden  
Telephone: +46 (0)31-772 1000

Cover:  
Co-porphyrine surrounded by water

Chalmers Reproservice  
Gothenburg, Sweden 2014

Water Oxidation on Porphyrines: A First-principles Study

Adam Arvidsson

Department of Applied Physics

Chalmers University of Technology, Gothenburg 2014

### **Abstract**

Research on electrocatalysts for water oxidation into hydrogen and oxygen is of great importance in order to combat global warming and make sustainable technology more efficient and economically viable. This thesis studies water oxidation on a cobalt-porphyrine catalyst with density functional theory (DFT), using the Quantum ESPRESSO software. Reaction energies for the two different porphyrines: the porphyrine and the hangman-porphyrine in vacuum were calculated and found to be in agreement with previous results.

After addressing the question of how water affects the oxygen evolution reaction (OER) on porphyrines many new challenges were identified. Using ab-initio molecular dynamics with a temperature, configurations were sampled and the configurations of minimum energy were found. This resulted in an unexpected reaction energy landscape. The properties of the water in this model were further investigated by studying the diffusion and radial distribution function of bulk water. It turns out that water in this model is more mobile than expected and appears to be in a liquid phase even at a temperature of 50 K. The unexpected energy landscape is attributed to the water model due to its unphysical behaviour.

**Keywords:** DFT, Porphyrines, Water oxidation, OER



## Acknowledgements

First and foremost, thanks to my supervisor Anders Hellman for all the help and guidance through this work.

Henrik Grönbeck for showing interest and offering useful advice.

My officemate Jenny for all feedback and for being open for all sorts of questions.

The rest of the Chemical Physics group for creating a good atmosphere.

Erik J, Erik F and Johannes for inputs and willingness to always discuss physics, programming and feedback on the report.

Johan for being most helpful trying to solve many problems.

Thanks to the supercomputer centre at Chalmers, C3SE, for the calculations and support.

Adam Arvidsson, Göteborg, 2014-05-30



# Contents

<b>1</b>	<b>Introduction</b>	<b>1</b>
1.1	Background . . . . .	1
<b>2</b>	<b>Catalysis and Water Oxidation</b>	<b>3</b>
2.1	Catalysis . . . . .	3
2.1.1	Sabatier's Principle - Volcano Plot . . . . .	4
2.2	Water Oxidation . . . . .	5
2.2.1	Scaling Relations . . . . .	7
2.2.2	Zero Point Energy Correction . . . . .	8
2.2.3	Reaction Energies . . . . .	8
2.2.4	Overpotential . . . . .	11
2.2.5	Solvent Correction . . . . .	12
2.3	Porphyrines . . . . .	12
<b>3</b>	<b>Density Functional Theory</b>	<b>15</b>
3.1	The Schrödinger Equation . . . . .	15
3.2	Hohenberg-Kohn Theorem . . . . .	16
3.3	Kohn-Sham Approach . . . . .	17
3.4	Exchange-Correlation Functional . . . . .	19
3.5	Ab-initio Molecular Dynamics . . . . .	20
<b>4</b>	<b>Computational Methods</b>	<b>23</b>
4.1	Calculation Scheme . . . . .	23
4.2	Parameters . . . . .	24
4.3	Plane Wave Basis Set . . . . .	25
4.4	Pseudopotentials . . . . .	25
4.5	Nosé-Hoover Thermostat . . . . .	27
4.6	Mean Square Displacement (MSD) . . . . .	27
4.7	Radial Distribution Function (RDF) . . . . .	28

<b>5</b>	<b>Results</b>	<b>29</b>
5.1	Co-porphyrine in Water . . . . .	29
5.1.1	Description of water . . . . .	33
5.1.2	Another Nosé-Hoover thermostat frequency . . . . .	35
<b>6</b>	<b>Discussion</b>	<b>36</b>
6.1	CoP in Water . . . . .	36
6.2	Water Model . . . . .	37
<b>7</b>	<b>Conclusions</b>	<b>39</b>
	<b>Bibliography</b>	<b>43</b>

# 1

## Introduction

ONE OF THE GREATEST challenges of today is to reduce our dependence on fossil fuels. Hydrogen as energy carrier and low-temperature fuel cell technology is an appealing alternative to the conventional combustion engine. One shortcoming of the present technology is the substantial overpotential at the oxygen electrodes and thus the large energy loss of the fuel cells. To this end research on electrocatalysts for water oxidation into hydrogen and oxygen is of great importance in order to make sustainable technology more efficient and economically viable. One recent path is to try and develop cheap catalysts inspired by biological systems such as enzymes and respiratory systems [1, 2]. Advances in DFT and computational power presents the ability to, via simulations on the atomic level, predict and design better catalysts [3].

This thesis has been about studying water oxidation on a porphyrine catalyst using DFT.

### 1.1 Background

In the hydrogen economy fossil fuels are replaced by hydrogen as a clean and sustainable energy carrier. Renewable energy sources are used to produce hydrogen via water splitting. When hydrogen is combusted, e.g. in a fuel cell, the only combustion product is water. One of the shortcomings of this technology today is the inefficiency of water splitting. Water is a very stable molecule and it requires quite a lot of energy to break it. To make this energy cost as small as possible research on suitable catalysts is ongoing.

In the previous work by Baran et al. [2] DFT simulations were performed on porphyrine

catalysts for different transition metals at the active site. However, the impact of a solvent around the reaction site was not simulated directly but approximated by making a simple correction based on how many hydrogen bonds the different intermediates can form and the average energy of such a bond. The focus of this study is to either confirm or disconfirm that approximation. In this project the same catalytic reaction will be studied trying to find the optimal configuration of water surrounding the active site directly by including water in the calculations.

# 2

## Catalysis and Water Oxidation

**I**N THIS CHAPTER the basics of catalysis and the electrochemical framework for the water oxidation reaction will be described and finally a brief description of porphyrines.

### 2.1 Catalysis

Catalysis is of immense importance to industry and society. A catalyst works by accelerating a chemical reaction which may otherwise be slow or even impossible. It is important to point out that a catalyst is not consumed during the reaction. It simply changes the conditions for said reaction and presents an alternative reaction mechanism by forming bonds with the reactants, allowing these to react and form a product on the catalyst. Then the product detaches from the catalyst leaving it unaltered and ready for the next reaction. This is illustrated in figure 2.1 where the reactants A and B bind to the catalyst and form the product P which then detaches from the catalyst surface.

Familiar examples of catalysis can be found in every-day life, for example in the after-treatment system found in almost all vehicles, where catalyst cleans the exhaust from amongst others poisonous carbon monoxide and nitrogen oxides. In chemical industry a substantial portion of all products are made in some form of catalytic process. One example is the iron-based catalyst used in the Haber-Bosch process, which enables mass production of fertilizers to feed the continuously growing population of our planet [5, 6]. These are examples of heterogeneous catalysis where the reactants and the catalysts are in different phases. In this type of catalysis the catalyst is often a surface and the reactants gases or liquids.

Another possibility is homogeneous catalysis, where both the reactants and the catalyst

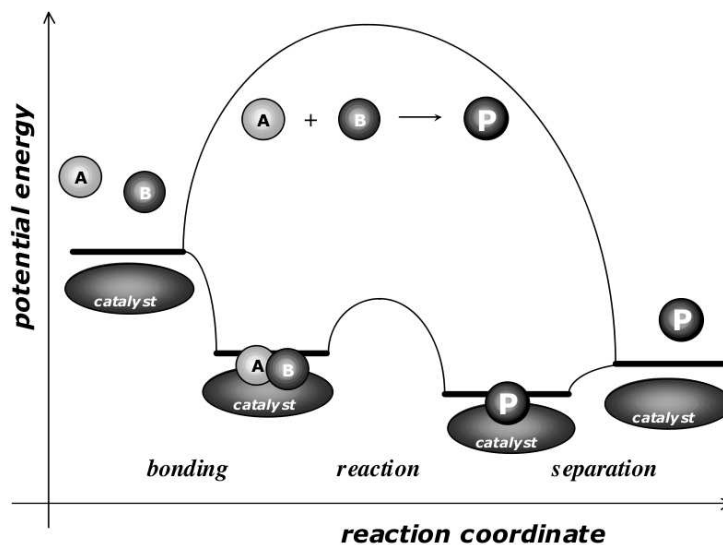


**Figure 2.1:** Illustration of catalysis reprinted with permission from [4]. The catalyst presents an alternative reaction route to the same end-product. It does so by binding the reactants A and B, which react in the adsorbed phase and form the product P on the surface of the catalyst. The product then detaches from the catalyst and leaves it ready for a new pair of reactants to land and begin the process over again. Copyright (2014) John Wiley and Sons.

are in the same phase, i.e. all constituents are molecules in the gas phase or in the liquid phase. In industry homogeneous catalysis is frequent in all kinds of reactions to produce chemicals.

In nature many interesting catalysts exist, e.g. enzymes. These are highly efficient catalysts often operating by matching the shape of the substrates or the transition state of the reaction they bind to. Enzymes represents a great source of inspiration for catalytic design.

### 2.1.1 Sabatier's Principle - Volcano Plot

Catalytic reactions proceed best if the interaction between the adsorbates and the catalyst is neither too strong, so the catalyst is poisoned and the reaction stops, nor too weak so the reaction never occurs in the first place [4]. Sabatier realised that there must be an optimum of the catalytic rate [7] and formulated what we now call Sabatier's principle. This is usually illustrated in a so called volcano plot where the rate is plotted against a descriptor for different catalysts. An example of a volcano plot is shown in figure 2.2 where the example is the decomposition of formic acid using different transition metals as catalysts. Here the heat of formation of the reaction intermediate is used as

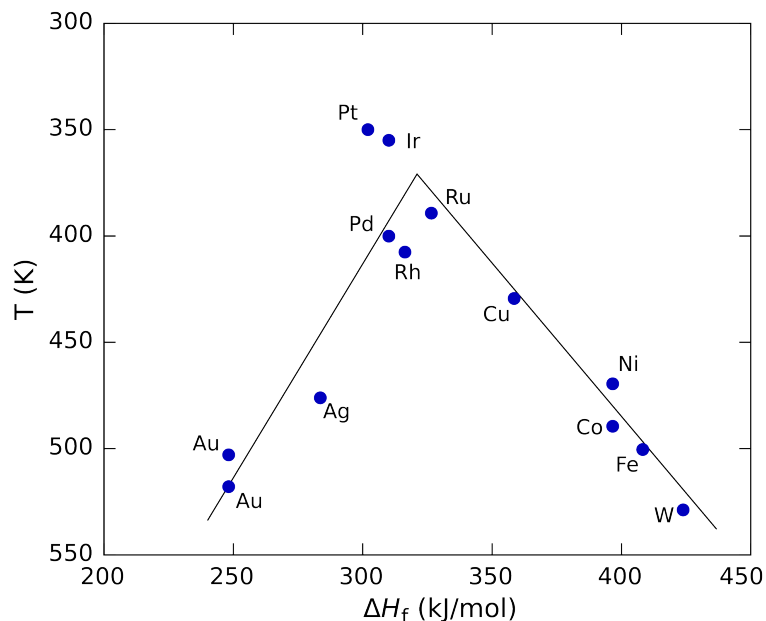
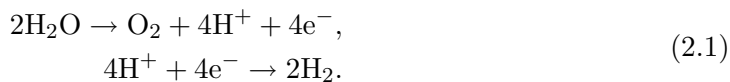


**Figure 2.2:** Example of a volcano plot for the decomposition of formic acid on transition metals taken from Wikipedia [8]. The activity (y-axis) is here described by the temperature at which the reaction reaches a specific rate. The descriptor is here the heat of formation (x-axis).

descriptor (horizontal axis). On the vertical axis the temperature at which the reaction reaches a specific rate is plotted in reverse, i.e. low temperature corresponds to a higher performance since less energy is needed for the same rate. At low heat of formation the reaction is too slow because the rate of adsorption is slow and rate-limiting and at high values desorption becomes the rate-limiting step. The maximum rate, which in this example is observed for metals in the platinum group, is observed for intermediate values.

## 2.2 Water Oxidation

Water oxidation is the reaction when water is split into hydrogen and oxygen



This reaction is endothermic, i.e. it requires energy to initiate it. But, since hydrogen gas is of interest we would like to achieve it non the less. One possibility is to use electrochemistry where we consider electrodes submerged in a solution of water and apply a voltage to force the reaction to take place. By using the theoretical framework

of the standard hydrogen electrode (SHE) as established by Nørskov et al. [9] it is possible to address this from first-principles. The equilibrium potential  $U = 0$  V is defined as when the free energies of  $1/2\text{H}_2(g)$  and  $\text{H}^+(aq) + e^-$  are equal, i.e.



With this definition adsorption is described as usual



where  $*H$  denotes an adsorbed hydrogen atom. However, the reference makes it easy to describe proton + electron reactions. Since the chemical potential of an electron is changed by a factor of  $-eU$  with respect to  $\text{H}_2$  in the gas phase, the free energy at potential  $U$  is changed according to

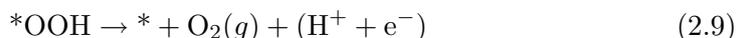
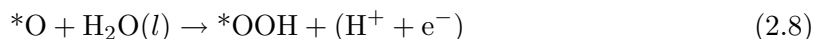
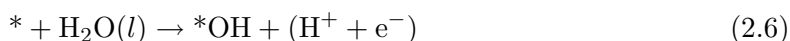
$$\Delta G(U) = \Delta G_0 + eU \quad (2.4)$$

where  $\Delta G_0$  is the free energy of the reaction when  $U = 0$  V. If there are  $n$  electrons involved the change will be  $neU$ . The Gibbs free energy can be calculated straightforwardly as

$$\Delta G_0 = \Delta E + \Delta \text{ZPE} - T\Delta S \quad (2.5)$$

where  $\Delta E$  is the total energy difference obtained from DFT calculations,  $\Delta \text{ZPE}$  is the change in zero point energy and  $\Delta S$  the change in entropy at temperature  $T$ . This will be used and explained later on.

When it comes to water oxidation and more specifically the oxygen evolution reaction (OER), we usually describe it as follows. All intermediates in the energy landscape are described as single proton transfers. In this way the oxygen evolution reaction  $2\text{H}_2\text{O} \rightarrow \text{O}_2 + 4(\text{H}^+ + e^-)$  is split into four electrochemical steps



where  $*$  denotes a free adsorption site and the  $*OH$  intermediate is OH chemisorbed on such a site. In each step a proton-electron pair is subtracted from the reactants and  $\text{H}_2\text{O}$  molecules are transformed into  $*OH$ ,  $*O$ ,  $*OOH$  and gas-phase  $\text{O}_2$  subsequently. Note that the proton and electron transfers are assumed to take place simultaneously.

Recombination of adsorbed oxygen atoms to  $\text{O}_2$ , i.e.  $*O + *O \rightarrow \text{O}_2$ , is not considered since this process can be expected to have a large activation barrier [10]. Only steps involving charge transfer are considered, which depend directly on the applied potential.

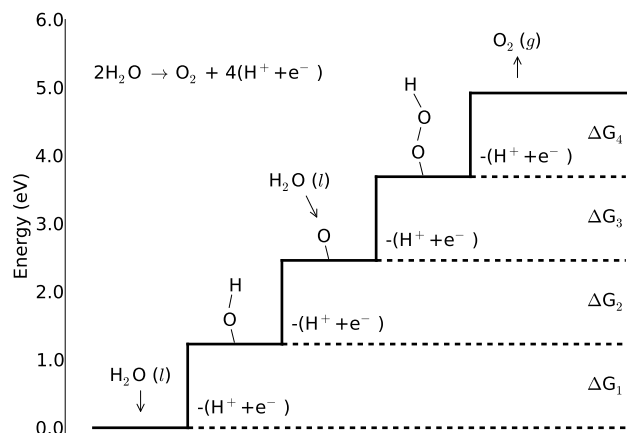


**Figure 2.3:** The oxygen evolution reaction for an ideal catalyst where all steps are 1.23 eV. In each step a proton-electron pair is subtracted from the reactants and  $\text{H}_2\text{O}$  molecules are transformed into  $\text{*OH}$ ,  $\text{*O}$ ,  $\text{*OOH}$  and gas-phase  $\text{O}_2$  subsequently. The figure is inspired by Calle-Vallejo et al. 2012 [11].

### 2.2.1 Scaling Relations

Experimentally it is known that the opposite to the OER, the oxygen reduction reaction (ORR), is exothermic by 4.92 eV at standard temperature and pressure<sup>1</sup>, i.e.



The OER is, of course, endothermic by the same amount. An ideal four-step process would then divide this energy gain in four and each step would be exothermic by 1.23 eV, which is illustrated in figure 2.3. However, this is not the case. Several recent studies have shown a constant energy difference between the  $\text{*OH}$  and the  $\text{*OOH}$  intermediates around 3.2 eV [2, 11] regardless of which catalyst is considered. This is usually explained with the idea that a surface is in this instance near-sighted and experience  $\text{*OH}$  and  $\text{*OOH}$  the same. The surface mostly experience the nearest adsorbed oxygen atom, and whether there is just one H or an OH beyond that does not change the interaction with the surface significantly.

Since the total energy toll must still be 4.92 eV this means that there must be a step larger than 1.23 eV, regardless of where the step between the the  $\text{*OH}$  and  $\text{*OOH}$  intermediates is placed. This is illustrated in figure 2.4. The strive is however to find a catalyst where this extra energy, or overpotential, is as small as possible.

In figure 2.5 we observe this scaling relation. By plotting the free energy for all intermediates for different catalysts (here different metals for the active sites has been

<sup>1</sup>25 °C and 1 atm, see pp. 152-153 in [12]

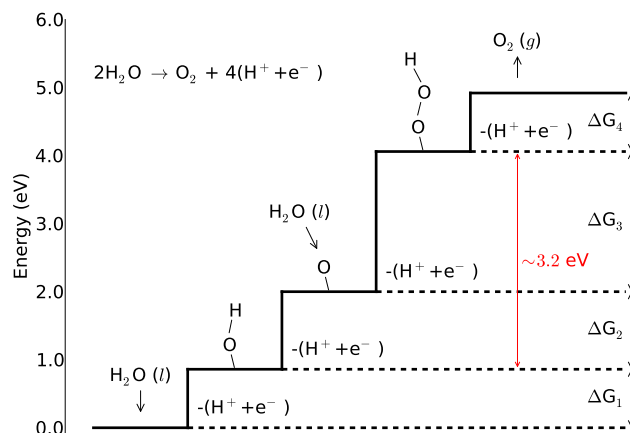


**Figure 2.4:** The reaction ladder when we take into account the observed scaling relation between the  $\text{*OH}$  and  $\text{*OOH}$  intermediates. This means that there has to be a step larger than the ideal 1.23 eV. How much larger is what we define as the overpotential which we would like to minimize.

varied) against the energy for the  $\text{*OH}$  intermediate we can linearise these and observe a constant difference between the  $\text{*OH}$  and  $\text{*OOH}$  energies. This is taken from the work by Baran et al. [2]. These lines are also what will make the lines in the corresponding volcano plot for this reaction (see figure 2.7).

## 2.2.2 Zero Point Energy Correction

For the free energies of the reaction steps we have to make a zero point energy (ZPE) correction. This is made since the quantum ground state have a finite energy in a harmonic potential. To a first approximation the atoms experience a harmonic potential. We can remind ourselves of the energy levels of the quantum harmonic oscillator

$$E_n = \hbar\omega\left(n + \frac{1}{2}\right), \quad (2.11)$$

which for it's ground state  $n = 0$  has a finite energy of  $1/2\hbar\omega$ . This is also illustrated in figure 2.6. This finite ground state energy or ZPE is not available for reactions and we have to take this into account.

## 2.2.3 Reaction Energies

Free energies for OER are calculated according to Calle-Vallejo et al. [11] and the zero point energy correction and the entropic contribution are taken from Nørskov et al. [9].

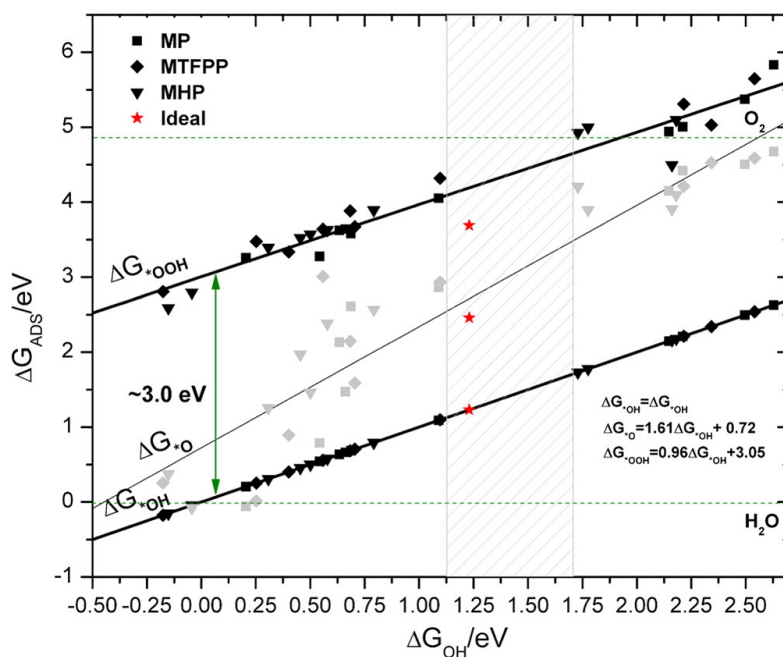


**Figure 2.5:** Adsorption energies for water oxidation on metal porphyrines (MP), metal hantman-porphyrines (MHP) and the metaltetrafluorophenylporphyrines (MTFPP) for different metals at the catalytically active site. Scaling relation is observed between the  $^*OH$  and  $^*OOH$  intermediate, i.e. a constant energy difference. Reprinted with permission from Baran et al. [2]. Copyright (2014) American Chemical Society.

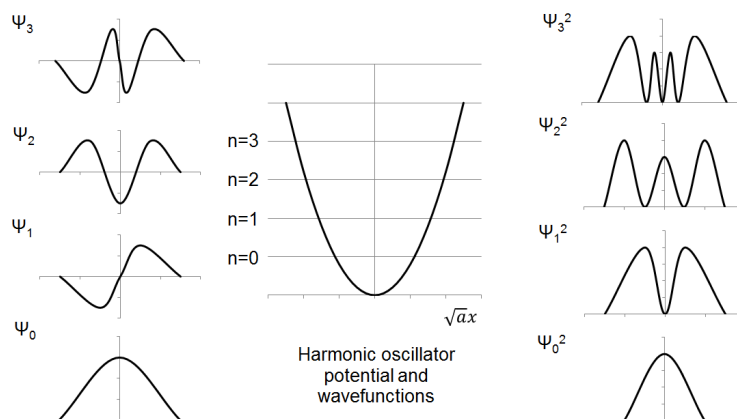


**Figure 2.6:** The quantum harmonic oscillator have a finite ground state energy  $n = 0$ . This is the zero point energy we have to subtract from the total energy calculated with DFT. Reprinted from Wikimedia [13].

According to Baran et al. [2] only small differences to these corrections are expected for the porphyrine systems and the literature values are therefore judged good enough. The energies are defined as

$$G^* = E_*^{\text{DFT}}, \quad (2.12)$$

$$G^*_{\text{OH}} = E^{\text{DFT}}_{*\text{OH}} + \text{ZPE}^*_{\text{OH}} - TS^*_{\text{OH}}, \quad (2.13)$$

$$G^*_\text{O} = E^{\text{DFT}}_{*\text{O}} + \text{ZPE}^*_{\text{O}} - TS^*_{\text{O}}, \quad (2.14)$$

$$G^*_{\text{OOH}} = E^{\text{DFT}}_{*\text{OOH}} + \text{ZPE}^*_{\text{OOH}} - TS^*_{\text{OOH}}, \quad (2.15)$$

and the reference energies are defined as

$$G_{\text{H}_2\text{O}} = E^{\text{DFT}}_{\text{H}_2\text{O}} + \text{ZPE}_{\text{H}_2\text{O}} - TS_{\text{H}_2\text{O}}, \quad (2.16)$$

$$G_{\text{H}_2} = E^{\text{DFT}}_{\text{H}_2} + \text{ZPE}_{\text{H}_2} - TS_{\text{H}_2}, \quad (2.17)$$

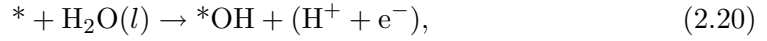
$$G_{\text{O}_2} = 4.92 \text{ eV} + 2(G_{\text{H}_2\text{O}} - G_{\text{H}_2}). \quad (2.18)$$

Defining  $G_{\text{O}_2}$  in this way ensures that the total energy difference for the sum of all steps is the same as the experimental value 4.92 eV, i.e.  $\Delta G_1 + \Delta G_2 + \Delta G_3 + \Delta G_4 = 4.92 \text{ eV}$  (see definitions below).

For the different steps the reaction energies are calculated by taking the difference between Gibbs free energy for the current and the previous step. Here we use the fact that we have defined that  $(\text{H}^+ + \text{e}^-) \rightleftharpoons 1/2\text{H}_2$  and consequently that

$$G_{(\text{H}^+ + \text{e}^-)} = 1/2 G_{\text{H}_2}. \quad (2.19)$$

The first step is a free water molecule reduced to an adsorbed \*OH



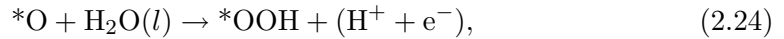
$$\Delta G_1 = G^*_{\text{OH}} + 1/2 G_{\text{H}_2} - (G^* + G_{\text{H}_2\text{O}}), \quad (2.21)$$

in the second step \*OH is reduced to \*O



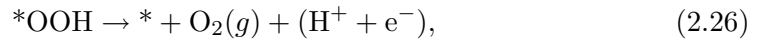
$$\Delta G_2 = G^*_\text{O} + 1/2 G_{\text{H}_2} - G^*_{\text{OH}}, \quad (2.23)$$

the third step reduces another water molecule on top of \*O



$$\Delta G_3 = G^*_{\text{OOH}} + 1/2 G_{\text{H}_2} - (G^*_\text{O} + G_{\text{H}_2\text{O}}), \quad (2.25)$$

and the fourth and last step gives oxygen by reducing \*OOH



$$\Delta G_4 = G^* + G_{\text{O}_2} + 1/2 G_{\text{H}_2} - G^*_{\text{OOH}}, \quad (2.27)$$

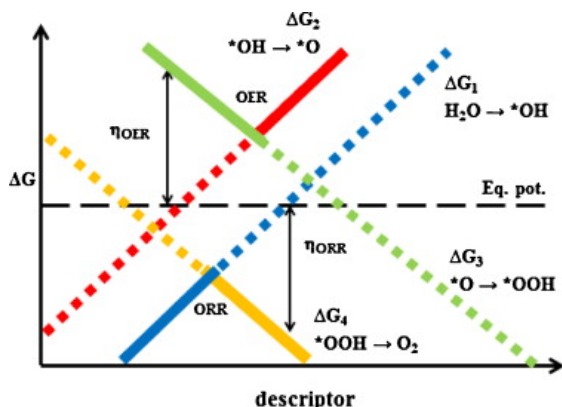


**Figure 2.7:** Oxygen evolution and reduction volcano plots reprinted from [11], Copyright (2014), with permission from Elsevier. The descriptor in our case would be  $\Delta G_1$ , the relative energy for the  $*\text{OH}$  intermediate. The distance to the equilibrium potential, the overpotential  $\eta$ , is a measurement of activity of the reaction.

These steps are all illustrated in figure 2.3.

Gibbs free energies for the OER are related to the ORR by considering the reaction in the other direction, by using 4.92 eV as reference. Since this thesis work is about water oxidation, i.e. OER, the steps are labelled from 1 - 4 for that reaction and are consistently called that also for the ORR.

Using the definitions above we can construct a volcano plot for the oxygen evolution and reduction reactions. This is illustrated in figure 2.7. The descriptor in our case would be  $\Delta G_1$ , the energy for the  $*\text{OH}$  intermediate because of the linear fits that was made by Baran et al. [2] (figure 2.5). The overpotentials  $\eta$  for the OER and the ORR, i.e. the difference from the equilibrium potential will be explained further in the following section.

## 2.2.4 Overpotential

The thermodynamic overpotential is an important parameter which is used to characterise the catalysts performance. It is defined as the maximum (or minimum) difference compared to the theoretical thermodynamical equilibrium potential, the "thermodynamically least favourable reaction step", or the potential-determining step (which is not necessarily the same as the rate-determining step) [14]. For example, in the OER case the overpotential is defined as the difference between the largest step<sup>2</sup> and the theoretical equilibrium potential value  $U_0 = 1.23 \text{ V}$ , i.e.

$$\eta^{\text{OER}} = U_0 - \max(\Delta G_1, \Delta G_2, \Delta G_3, \Delta G_4)/e. \quad (2.28)$$

This is the theoretical minimum voltage we have to apply to start the reaction. It could still not be enough since we have discarded any activation barriers that may occur here.

<sup>2</sup>by dividing the energies in eV with the electronic charge  $e$  we get the corresponding potential in volts

For the reduction reaction (ORR) the overpotential is defined as the difference between the smallest step and the theoretical value, i.e.

$$\eta^{\text{ORR}} = U_0 - \min(\Delta G_1, \Delta G_2, \Delta G_3, \Delta G_4)/e. \quad (2.29)$$

This can be viewed as how much we can decrease the applied potential and still (just) get the reaction to spontaneously occur (provided that there are no large activation barriers).

### 2.2.5 Solvent Correction

In the previous work without solvent by Baran et al. [2], a solvent correction was added to the reaction energies. This correction is described by Calle-Vallejo et al. 2011 [15] to account for the energy contribution that arise from hydrogen bonds between the \*OH and \*OOH adsorbates and the surrounding water molecules. The additional hydrogen bond energy has been experimentally established to be  $\sim 0.15$  eV per such bond. Since \*OH and \*OOH are able to form two hydrogen bonds on the simple porphyrine, a correction of  $2G_w = 0.30$  eV was made. The \*O intermediate and the free porphyrine can on the other hand not form such hydrogen bonds. This means that equations (2.13) and (2.15) are modified to

$$G_{*\text{OH}} = E_{*\text{OH}}^{\text{DFT}} + \text{ZPE}_{*\text{OH}} - TS_{*\text{OH}} + 2G_w \quad (2.30)$$

$$G_{*\text{OOH}} = E_{*\text{OOH}}^{\text{DFT}} + \text{ZPE}_{*\text{OOH}} - TS_{*\text{OOH}} + 2G_w \quad (2.31)$$

However, the hanging carboxylic group on the hangman-porphyrine already provides a hydrogen bond to the adsorbate. Thus, a correction of one  $G_w = 0.15$  eV was made for the hangman-porphyrine. The usage of this correction is what we would like to confirm or disconfirm by adding water around the porphyrine-complexes and finding the configuration of minimum energy by letting the system respond to the water.

## 2.3 Porphyrines

The base of a porphyrine molecule is a cyclic platform stabilized with delocalized electrons in a carbon ring. In many instances porphyrines have a central metal atom coordinated to four nitrogen atoms. As catalysts, this metal atom is the active reaction site. Apart from the simple metal-porphyrine (to the left in figure 2.8) there exists many naturally occurring porphyrines in various forms with various side groups. One form which has recently been synthesised is the hangman-porphyrine [16, 17] (to the right in figure 2.8) which was studied in vacuum in this thesis. This molecule has different side groups attached to the porphyrine platform, including a hangman scaffold with a carboxylic acid group hanging above the central metal atom. The basic structure of the cobalt-porphyrine and the cobalt-hangman-porphyrine can be seen in figure 2.8.

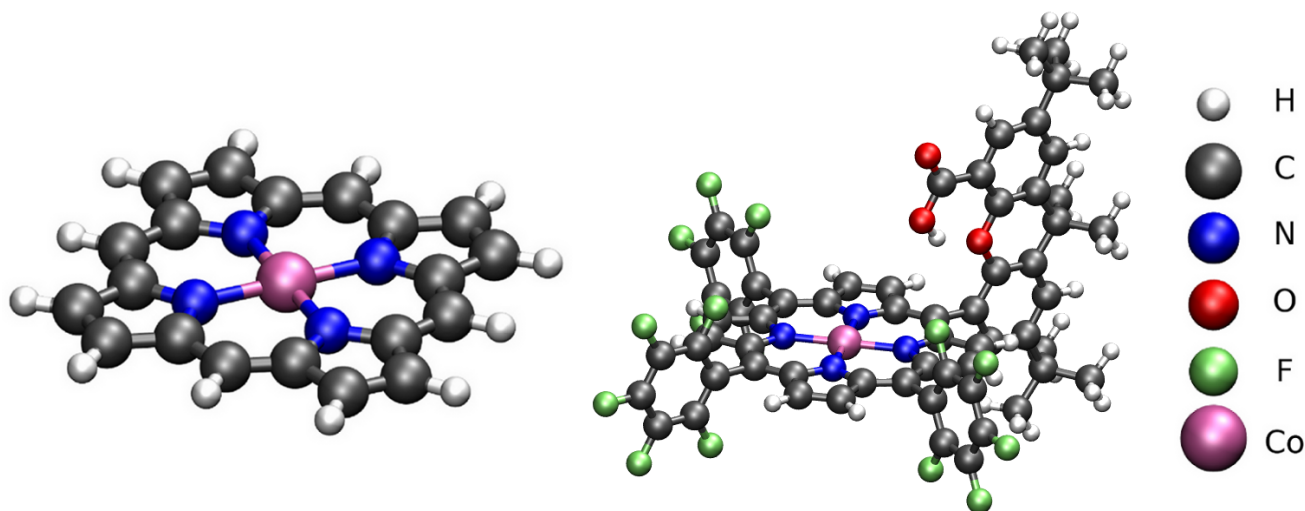


**Figure 2.8:** Structure of the Co-porphyrine (left) and the Co-hangman-porphyrine (right).

In the article by Baran et al. [2], different transition metals were investigated for the active site of the porphyrine and two other porphyrine-based molecules, the hangman-porphyrine and metaltetrafluorophenyloporphyrines. This is summarised in the volcano plot in figure 2.9. In accordance with experimental observations [17] it was found that cobalt (Co) was by far the best metal for the active site. This is why Co was chosen as the active metal atom in this work.

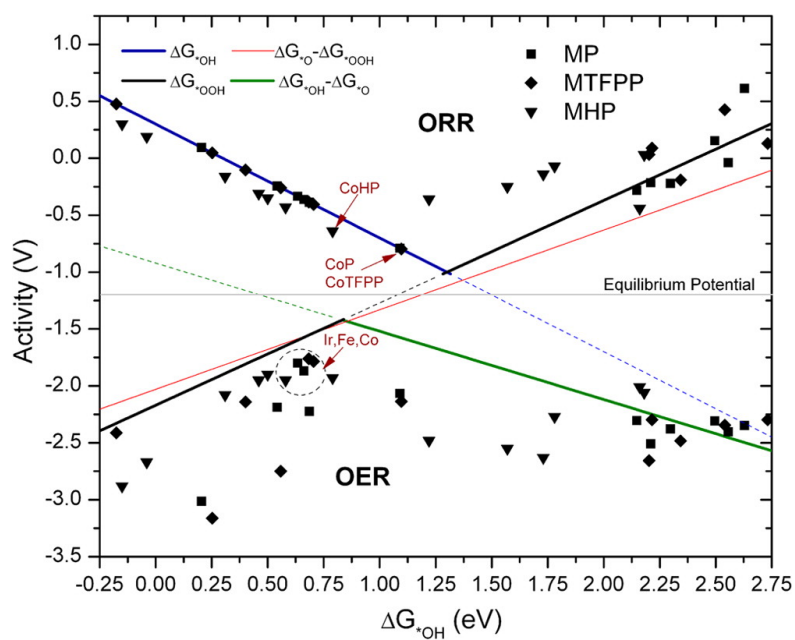


**Figure 2.9:** Volcano plot for different transition metals centers for the metal porphyrine (MP), the metal hangerman-porphyrine (MHP) and the metaltetrafluorophenylporphyrines (MTFPP). Reprinted with permission from Baran et al. [2]. Copyright (2014) American Chemical Society.

# 3

## Density Functional Theory

A WIDESPREAD TOOL in computational chemical physics is Density Functional Theory (DFT). It is a way to describe a many-particle system from first principle by rewriting the Schrödinger equation in a clever way. This will be further explained in the following chapter.

### 3.1 The Schrödinger Equation

The stationary Schrödinger equation [18] reads

$$\hat{H}\Psi = E\Psi, \quad (3.1)$$

where  $\hat{H}$  is the Hamiltonian and  $E$  the total energy of the system. The solution to this equation gives us the total wave function  $\Psi$  which in principle contains all wanted properties of the system and is therefore essential in quantum mechanics. The goal is therefore to find this wave function or equivalently, as in the case of DFT, the density  $n(\mathbf{r}) = |\Psi|^2$ .

For the many-body problem of a system containing  $N$  electrons and  $K$  nuclei with charge  $Z_I$  the Hamiltonian reads [19, 20]

$$\begin{aligned} \hat{H} = & - \sum_{i=1}^N \frac{\hbar^2}{2m_e} \nabla_i^2 - \sum_{I=1}^K \frac{\hbar^2}{2M_I} \nabla_I^2 + \frac{1}{4\pi\epsilon_0} \sum_{i=1}^N \sum_{j>i}^N \frac{e^2}{|\mathbf{r}_i - \mathbf{r}_j|} \\ & - \frac{1}{4\pi\epsilon_0} \sum_{I=1}^K \sum_{i=1}^N \frac{Z_I e^2}{|\mathbf{r}_i - \mathbf{R}_I|} + \frac{1}{4\pi\epsilon_0} \sum_{I=1}^K \sum_{J>I}^K \frac{Z_I Z_J e^2}{|\mathbf{R}_I - \mathbf{R}_J|}. \end{aligned} \quad (3.2)$$

This looks rather complicated. It turns out that the stationary Schrödinger equation can only be solved analytically for a one-electron system, e.g. the hydrogen atom or the ionized helium atom  $\text{He}^+$ . So, to be able to continue, certain approximations have to be made. As a first approximation one usually makes the Born-Oppenheimer approximation [21] which is justified by the fact that the nuclei (ions) are much heavier than the electrons,  $M_I \gg m_e$ . In most cases, this justifies a time-scale separation by saying that the electrons immediately adapt to changes in the positions of the ions. This means that the electronic and ionic system can be treated separately and for the electrons the ions can be regarded as fixed. We can therefore drop the ionic kinetic energy term and the ion-ion interaction term in the Hamiltonian and only consider the terms involving electrons

$$\hat{H}_{\text{BO}} = - \sum_{i=1}^N \frac{\hbar^2}{2m_e} \nabla_i^2 + \frac{1}{4\pi\epsilon_0} \sum_{i=1}^N \sum_{j>i}^N \frac{e^2}{|\mathbf{r}_i - \mathbf{r}_j|} - \frac{1}{4\pi\epsilon_0} \sum_{I=1}^K \sum_{i=1}^N \frac{Z_I e^2}{|\mathbf{r}_i - \mathbf{R}_I|}. \quad (3.3)$$

If we denote the interaction of electron  $i$  with the ions  $V_{\text{ext}}(\mathbf{r}_i)$  and use Hartree atomic units  $\hbar = m_e = e = 1/(4\pi\epsilon_0) = 1$ , we can write the Hamiltonian as<sup>1</sup>

$$\hat{H} = -\frac{1}{2} \sum_i \nabla_i^2 + \sum_i \sum_{j>i} \frac{1}{|\mathbf{r}_i - \mathbf{r}_j|} + \sum_i V_{\text{ext}}(\mathbf{r}_i). \quad (3.4)$$

With this Hamiltonian the problem is still very computationally expensive to solve for more than a few electrons.

## 3.2 Hohenberg-Kohn Theorem

We can now use the theory laid out by Hohenberg and Kohn in 1964 [22]. They proved that  $V_{\text{ext}}(\mathbf{r})$  is uniquely determined by the ground state electron density  $n_0(\mathbf{r})$  and that you can write the energy as a functional of the electron density  $n(\mathbf{r}) = |\Psi|^2$  which is minimised by the ground state. In other words, while the Schrödinger equation (3.1) gives us a way to construct the density from the potential

$$V_{\text{ext}} \rightarrow \Psi \rightarrow n \quad (3.5)$$

Hohenberg and Kohn tell us how to go from the density to the potential, to the wave function which describes everything in the system

$$n \rightarrow V_{\text{ext}} \rightarrow \Psi \rightarrow \text{everything!} \quad (3.6)$$

This means that the density uniquely determines  $V_{\text{ext}}$ , which has a unique ground state  $\Psi_0$ , and thus in principle, we know everything from the density. This means that we can rewrite the whole problem in terms of the electron density  $n(\mathbf{r})$ . This is very helpful since

<sup>1</sup>without the index on  $\hat{H}_{\text{BO}}$  to simplify things

we then only have to store one number (the density) per point in space instead of the total wave function  $\Psi$  which depends on the coordinates of all electrons. Furthermore we can use the variational principle to obtain the ground state [23].

According to the variational principle the ground state energy is

$$E_0 \leq E = \frac{\langle \Psi | \hat{H} | \Psi \rangle}{\langle \Psi | \Psi \rangle} \quad (3.7)$$

or assuming the wave function to be normalised  $\langle \Psi | \Psi \rangle = 1$

$$E_0[n] = \min_n \langle \Psi | \hat{H} | \Psi \rangle = \min_n \left[ \mathcal{F}[n] + \int n(\mathbf{r}) V_{\text{ext}}[n(\mathbf{r})] \, \mathbf{dr} \right] \quad (3.8)$$

since the total wave function  $\Psi$  is a functional of the density  $\Psi = \Psi[n(\mathbf{r})]$ . Here  $\mathcal{F}[n]$  includes all internal energies, kinetic and potential, and  $V_{\text{ext}}$  is the external potential due to the ions. We can utilise the variational principle in order to obtain the lowest energy by iteration. The remaining problem is how to describe the many-particle wave function  $\Psi$  or the density  $n(\mathbf{r})$ .

This far we know that it is a good idea and that it is possible to consider the problem in terms of the electron density  $n(\mathbf{r})$  and that it is possible to obtain the ground state energy, which is the minimum energy by the variational principle, by iteration. To proceed we need the work by Kohn and Sham.

### 3.3 Kohn-Sham Approach

What Kohn and Sham did in their work from 1965 [24] was to make the ansatz of an auxiliary system of independent particle orbitals  $\psi_i$  whose density

$$n(\mathbf{r}) = \sum_{i=1}^N \int \psi_i^*(\mathbf{r}) \psi_i(\mathbf{r}) \, \mathbf{dr} = \sum_{i=1}^N |\psi_i(\mathbf{r})|^2, \quad (3.9)$$

is the real density of the system. In equation (3.9) there are  $N$  occupied orbitals, i.e. have orbital energies  $\varepsilon_i$  below the fermi level. Kohn and Sham then rearranged the terms in the energy functional in a clever way, namely

$$E_{\text{KS}}[n] = T_0[n] + \int n(\mathbf{r}) V_{\text{ext}}[n(\mathbf{r})] \, \mathbf{dr} + E_{\text{H}}[n] + E_{\text{xc}}[n]. \quad (3.10)$$

Lumping together what we cannot describe exactly, the many-body effects, i.e. what we miss when we go from the full many-particle wave function  $\Psi$  to the independent one-particle orbitals  $\psi_i$ , and calling it *exchange-correlation* (xc). In equation (3.10), we have the first term which is the kinetic contribution from *non*-interacting electrons, the

second term we recognise as the interaction with the ions (let us from now on call it  $E_{\text{ext}}[n]$ ), and the third term

$$E_{\text{H}}[n] = \frac{1}{2} \int \int \frac{n(\mathbf{r})n(\mathbf{r}')}{|\mathbf{r} - \mathbf{r}'|} \mathrm{d}\mathbf{r} \mathrm{d}\mathbf{r}', \quad (3.11)$$

is the Hartree term which is a mean-field approximation, i.e. that each electron feels an average effect from all the other electrons. From this Kohn-Sham energy functional we can derive a set of equations we can use to find the electron density.

The Kohn-Sham equations can be derived by applying the variational principle on the Kohn-Sham energy functional

$$\frac{\delta E_{\text{KS}}}{\delta \psi_i^*(\mathbf{r})} = 0, \quad (3.12)$$

where  $\frac{\delta}{\delta \psi_i^*(\mathbf{r})}$  is a functional derivative. Under the orthonormalization constraint  $\langle \psi_i | \psi_j \rangle = \delta_{ij}$  and applying the chain rule we obtain

$$\begin{aligned} \frac{\delta T}{\delta \psi_i^*(\mathbf{r})} + \left[ \frac{\delta E_{\text{ext}}}{\delta n(\mathbf{r})} + \frac{\delta E_{\text{H}}}{\delta n(\mathbf{r})} + \frac{\delta E_{\text{xc}}}{\delta n(\mathbf{r})} \right] \frac{\delta n(\mathbf{r})}{\delta \psi_i^*(\mathbf{r})} \\ - \varepsilon_i \frac{\delta}{\delta \psi_i^*(\mathbf{r})} \left[ \int \psi_i^*(\mathbf{r}) \psi_i(\mathbf{r}) \mathrm{d}\mathbf{r} - 1 \right] = 0, \end{aligned} \quad (3.13)$$

where  $\varepsilon_i$  is the Lagrange multiplier for the constraint. Using the expression for  $T[n]$  we get

$$\frac{\delta T}{\delta \psi_i^*(\mathbf{r})} = \frac{\delta}{\delta \psi_i^*(\mathbf{r})} \left[ -\frac{1}{2} \sum_{i'} \int \psi_{i'}^*(\mathbf{r}) \nabla^2 \psi_{i'}(\mathbf{r}) \mathrm{d}\mathbf{r} \right] = -\frac{1}{2} \nabla^2 \psi_i(\mathbf{r}), \quad (3.14)$$

from the expression for  $E_{\text{ext}}$  in equation (3.10) we get

$$\frac{\delta E_{\text{ext}}}{\delta n(\mathbf{r})} = \frac{\delta}{\delta n(\mathbf{r})} \left[ \int n(\mathbf{r}) V_{\text{ext}}(\mathbf{r}) \mathrm{d}\mathbf{r} \right] = V_{\text{ext}}(\mathbf{r}), \quad (3.15)$$

and in the same manner

$$\frac{\delta E_{\text{H}}}{\delta n(\mathbf{r})} = \int \frac{n(\mathbf{r}')}{|\mathbf{r} - \mathbf{r}'|} \mathrm{d}\mathbf{r}' \quad \text{and} \quad \frac{\delta}{\delta \psi_i^*(\mathbf{r})} \left[ \int \psi_i^*(\mathbf{r}) \psi_i(\mathbf{r}) \mathrm{d}\mathbf{r} \right] = \psi_i(\mathbf{r}). \quad (3.16)$$

Putting all of this into equation (3.13) we get the Kohn-Sham equations for the single-particle orbital  $\psi_i(\mathbf{r})$

$$-\frac{1}{2} \nabla^2 \psi_i(\mathbf{r}) + \left[ V_{\text{ext}}(\mathbf{r}) + \int \frac{n(\mathbf{r}')}{|\mathbf{r} - \mathbf{r}'|} \mathrm{d}\mathbf{r}' + \frac{\delta E_{\text{xc}}}{\delta n(\mathbf{r})} \right] \psi_i(\mathbf{r}) = \varepsilon_i \psi_i(\mathbf{r}). \quad (3.17)$$

A common way to write this is with an effective potential

$$\left( -\frac{1}{2} \nabla^2 + V_{\text{eff}} \right) \psi_i(\mathbf{r}) = \varepsilon_i \psi_i(\mathbf{r}), \quad (3.18)$$

where the effective potential  $V_{\text{eff}}$  is given by

$$V_{\text{eff}} = V_{\text{ext}}(\mathbf{r}) + \int \frac{n(\mathbf{r}')}{|\mathbf{r} - \mathbf{r}'|} d\mathbf{r}' + V_{\text{xc}}[n(\mathbf{r})], \quad (3.19)$$

where

$$V_{\text{xc}}[n(\mathbf{r})] = \frac{\delta E_{\text{xc}}[n]}{\delta n(\mathbf{r})}. \quad (3.20)$$

Provided that we can describe the exchange-correlation functional in a correct way this will give us the true density  $n(\mathbf{r})$ . It is important to point out that this transformation to an auxiliary system of one-particle orbitals, or Kohn-Sham orbitals,  $\psi_i$  is fundamentally different from the description of the many-body Schrödinger equation with the full many-body wave function  $\Psi$  and is made only to obtain the true density  $n(\mathbf{r})$ . The Kohn-Sham orbitals  $\psi_i$  and energies  $\varepsilon_i$  are mathematical constructions, and are not related to the "correct" wave function and have no intuitive physical meaning. There are however some relations to the real system. The eigenvalues are for example related to the total energy according to

$$E[n] = \sum_{i=1}^N \varepsilon_i - E_{\text{H}}[n] - \int n(\mathbf{r})V_{\text{xc}}[n(\mathbf{r})] d\mathbf{r} + E_{\text{xc}}[n]. \quad (3.21)$$

The ion-ion interaction energy is calculated separately and added to the total energy.

So, what a DFT implementation basically does is to solve the Kohn-Sham equations, i.e. solve the eigenvalue problems in equation (3.18) in a self-consistent way with an approximation to the exchange-correlation. Then various schemes and techniques can be used in different ways in different implementations, e.g. by moving the atoms along the forces which is given by the gradient of the energy [25] we can do a structural relaxation and find the equilibrium structure of the system.

### 3.4 Exchange-Correlation Functional

How to describe exchange and correlation exactly is unfortunately not known. There are, however, a number of approximation of increasing accuracy as well as computational cost [26]. Some of the most common will be presented below.

The simplest one is called the local density approximation (LDA) where we only consider the exchange and correlation energy to depend on the local density  $n(\mathbf{r})$

$$E_{\text{xc}}^{\text{LDA}} = \int n(\mathbf{r})\epsilon_{\text{xc}}[n(\mathbf{r}),\mathbf{r}] d\mathbf{r}, \quad (3.22)$$

where  $\epsilon_{\text{xc}}$  is the exchange-correlation energy density of the homogeneous electron gas. Taking spin into account we get the local spin density (LSD) approximation, i.e.

$$\epsilon_{\text{xc}}[n(\mathbf{r})] \longrightarrow \epsilon_{\text{xc}}[n_{\uparrow}(\mathbf{r}),n_{\downarrow}(\mathbf{r})]. \quad (3.23)$$

This is a reasonable first approximation and surprisingly good for many atoms and molecules [27].

Maybe the most commonly used exchange-correlation approximation is the next level of approximation, the generalized gradient approximation (GGA) where we take into account the gradient of the electron density as well

$$E_{\text{xc}}^{\text{GGA}} = \int n(\mathbf{r}) \epsilon_{\text{xc}}[\nabla n(\mathbf{r}), n(\mathbf{r}), \mathbf{r}] \, \text{d}\mathbf{r}. \quad (3.24)$$

The next level of approximations are the meta-generalized gradient approximation (meta-GGA), in which we can also include the kinetic energy of the Kohn-Sham orbitals  $\tau(\mathbf{r}) = \sum_{i=1}^N \frac{1}{2} |\nabla \psi_i(\mathbf{r})|^2$  or the second derivatives of the electron density  $\nabla^2 n(\mathbf{r})$ .

Then comes what is usually called hybrid functionals, where we use the exact exchange for the homogeneous electron gas (which we know from Hartree theory)

$$E_{\text{xc}}^{\text{hybrid}} = E_{\text{xc}}^{\text{GGA}} + a (E_{\text{x}}^{\text{exact}} - E_{\text{x}}^{\text{GGA}}), \quad (3.25)$$

where exact exchange is given by [28]

$$E_{\text{x}}^{\text{exact}} = -\frac{1}{2} \sum_{i,j} \int \int \frac{\psi_i^*(\mathbf{r}) \psi_j^*(\mathbf{r}') \psi_j(\mathbf{r}) \psi_i(\mathbf{r}')}{|\mathbf{r} - \mathbf{r}'|} \, \text{d}\mathbf{r} \, \text{d}\mathbf{r}'. \quad (3.26)$$

Higher levels of approximation often deal more explicitly with the correlation part of the functional.

In this work the GGA exchange-correlation functional proposed by Perdew, Burke, and Ernzerhof (PBE) [29] is used since it is quite common and yields a good compromise between accuracy and computational cost. Table 3.1 shows atomization energies for GGA compared to experimental values.

### 3.5 Ab-initio Molecular Dynamics

The Car-Parrinello method is a way to combine molecular dynamics and density functional theory [30]. This is done by reformulating the eigenvalue problem for the independent Kohn-Sham orbitals

$$\hat{H}_{\text{KS}} \psi_i = \epsilon_i \psi_i \quad (3.27)$$

and instead solving a virtual problem described by the Lagrangian [19, 30]

$$\begin{aligned} \hat{L} = & \sum_i \frac{1}{2} \mu \int |\dot{\psi}_i(\mathbf{r})|^2 \, \text{d}\mathbf{r} + \sum_I \frac{1}{2} M_I \dot{\mathbf{R}}_I^2 - E[\psi_i, \mathbf{R}_I] \\ & + \sum_{ij} \Lambda_{ij} \left[ \int \psi_i^*(\mathbf{r}) \psi_j(\mathbf{r}) \, \text{d}\mathbf{r} - \delta_{ij} \right] \end{aligned} \quad (3.28)$$

**Table 3.1:** Atomization energies of molecules in kcal/mol, which demonstrates that the PBE functional is better than the local spin density (LSD). Reprinted from [29]. Copyright (2014) by The American Physical Society.

System	$\Delta E^{\text{UHF}}$	$\Delta E^{\text{LSD}}$	$\Delta E^{\text{PW91}}$	$\Delta E^{\text{PBE}}$	$\Delta E^{\text{exp t}}$
H <sub>2</sub>	84	113	105	105	109
LiH	33	60	53	52	58
CH <sub>4</sub>	328	462	421	420	419
NH <sub>3</sub>	201	337	303	302	297
OH	68	124	110	110	107
H <sub>2</sub> O	155	267	235	234	232
HF	97	162	143	142	141
Li <sub>2</sub>	3	23	20	19	24
LiF	89	153	137	136	139
Be <sub>2</sub>	-7	13	10	10	3
C <sub>2</sub> H <sub>2</sub>	294	460	415	415	405
C <sub>2</sub> H <sub>4</sub>	428	633	573	571	563
HCN	199	361	326	326	312
CO	174	299	269	269	259
N <sub>2</sub>	115	267	242	243	229
NO	53	199	171	172	153
O <sub>2</sub>	33	175	143	144	121
F <sub>2</sub>	-37	78	54	53	39
P <sub>2</sub>	36	142	120	120	117
Cl <sub>2</sub>	17	81	64	63	58
Mean abs. error	71.2	31.4	8.0	7.9	...

where  $\mu$  and  $M_I$  are the fictitious masses of the electrons and the nuclei respectively.  $\Lambda_{ij}$  are Lagrange multipliers introduced in order to satisfy the constraint that  $\langle \psi_i | \psi_j \rangle = \delta_{ij}$ . From this Lagrangian we can obtain the equations of motion

$$\begin{aligned} \mu \ddot{\psi}_i(\mathbf{r}, t) &= -\frac{\delta E}{\delta \psi_i^*(\mathbf{r})} + \sum_k \Lambda_{ik} \psi_k(\mathbf{r}, t) \\ &= -\hat{H}_{\text{KS}} \psi_i(\mathbf{r}, t) + \sum_k \Lambda_{ik} \psi_k(\mathbf{r}, t) \end{aligned} \quad (3.29)$$

$$M_I \ddot{\mathbf{R}}_I = -\frac{\partial E}{\partial \mathbf{R}_I} \quad (3.30)$$

which can be solved with a standard verlet algorithm [31].  $E[\psi_i, \mathbf{R}_I]$  is the total energy within the DFT formalism (eq. (3.10)). This means that we can view the problem as a classical mechanics problem with the potential energy given by  $E[\psi_i, \mathbf{R}_I]$ . Hence we can apply any minimization algorithm to obtain the ground state. We can for instance do this by performing an initial annealing [32], i.e. slowly reducing the temperature, to find the equilibrium state of minimal energy.

When having reached the electronic ground state on the Born-Oppenheimer (BO) surface (where the BO approximation is valid), standard molecular dynamics can be applied to reach any finite temperature by solving the equations of motion given by the Lagrangian. To keep the system in the ground state (on the BO surface) it is important to choose the time step of the simulation sufficiently small.

The fictitious electronic mass  $\mu$  should be chosen such that the electronic wave functions adapt reasonably well to a change in the nuclear configuration. This means that it should be much smaller than the nuclear masses, but not so small that they take huge steps and leave the BO surface.

# 4

## Computational Methods

**T**O FIND THE OPTIMAL CONFIGURATION of water surrounding the porphyrine an ab-initio molecular dynamics simulation was run for the catalyst in a water solvent. This allows for a sampling of configurations. By studying the energy as a function of time the configuration of minimum energy can be found and further analysed.

The simulations were performed using the software Quantum ESPRESSO where the acronym ESPRESSO stands for opEn Source Package for Research in Electronic Structure, Simulation, and Optimization [33]. This code presents the possibility to do Car-Parrinello molecular dynamics (CP) and a standard plane wave code (PW) which allows for structural relaxation.

### 4.1 Calculation Scheme

The first step in the calculation scheme was to randomly distribute a number of water molecules around the porphyrine catalyst with all intermediates (eqs. (2.12) - (2.15)). This was done by placing 45 water molecules in a random orientation in a near-ellipsoidal shell around the catalytic complex in a cubic unit cell with dimensions  $20 \text{ \AA} \times 20 \text{ \AA} \times 10 \text{ \AA}$ . See figure 4.1. The structure of the porphyrine with intermediates was obtained by performing a structural relaxation with the PW code on the structures obtained by Baran et al. [2] without water molecules.

The next step was to run a structural relaxation (PW) on this system to get rid of the excess energy introduced by placing the water molecules in a random fashion.

In the third step, dynamics was applied using the CP code. First the ions were moved a

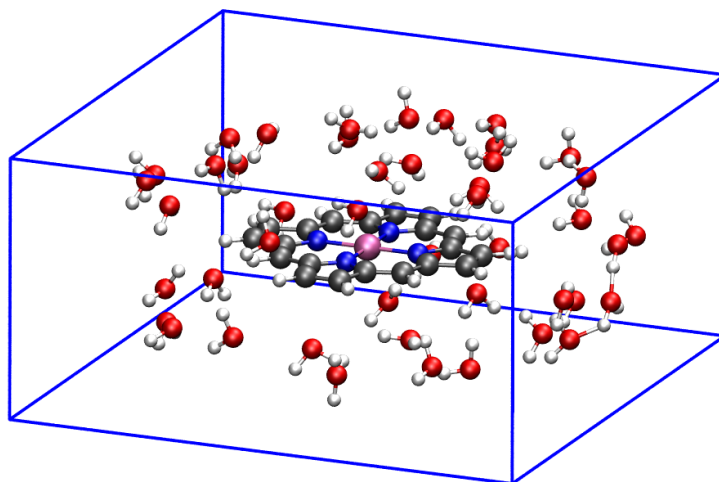


**Figure 4.1:** The initial structure with 45 water molecules placed in a near-ellipsoidal shell around the catalyst complex in a cubic unit cell with dimensions  $20 \text{ \AA} \times 20 \text{ \AA} \times 10 \text{ \AA}$ .

little and then kept fixed while the electrons were allowed to equilibrate. Then the equilibrated electronic system was subjected to a full dynamics simulation and a temperature of 50 K was applied for the ions.

By studying the energy as a function of time, the configuration of the apparent minimum energy was selected and subjected to another PW simulation to find its ground state at 0 K. These are the energies we can apply to equation (2.12) - (2.15).

## 4.2 Parameters

The time step was set to 2 a.u. (0.048 fs), which is quite short and thereby set some restrictions on how long the system could be evolved in time. The time step needed to be so short since nonphysical behavior was observed for larger values.

The fictitious electronic mass was set to 400 a.u., which is 400 times the real electron mass.

To enhance the separation of the electronic and ionic degrees of freedom it is customary to replace the mass of hydrogen by the mass of deuterium [34, 35]. This allows for a longer time step.

To be able to afford the computational cost, the number of water molecules set some re-

restrictions. Each water molecule introduces more electrons to the system which increases the number of equations to solve and thus the number of iterations needed to reach convergence. This is why a single shell of water around the porphyrine was studied and not a bulk water-like surrounding.

### 4.3 Plane Wave Basis Set

It is common to represent the Kohn-Sham orbitals using a plane-wave basis set, i.e. expanding the orbitals by determining the coefficients  $c_{\mathbf{k},\mathbf{G}}$  in

$$\psi_{\mathbf{k}}(\mathbf{r}) = \sum_{\mathbf{G}} c_{\mathbf{k},\mathbf{G}} e^{-i(\mathbf{k}+\mathbf{G})\cdot\mathbf{r}}. \quad (4.1)$$

There are some benefits and drawbacks to using this. It is advantageous to use when having periodic boundary conditions since the plane waves are periodic. Another benefit is that it constitutes a complete basis set. Any state can be expressed in terms of these. Quantum ESPRESSO uses periodic boundary conditions in all directions and employs a plane-wave basis.

One drawback is that you may need quite a few of these plane-waves to make an accurate representation. A plane wave expansion is usually truncated at an energy cutoff  $E_{\text{cut}}$ . This is to say that plane waves corresponding to energies higher than  $E_{\text{cut}}$  are disregarded and their coefficients are set to zero.

In the implementation of Quantum ESPRESSO it is possible to specify a cutoff energy for both the wave functions and for the density. These were chosen according to the recommended values for the pseudopotentials (see the section below) to 48 or 49 Ry ( $\sim 653$  eV or  $667$  eV) for the wave functions and 324 Ry for the density. These were confirmed by doing a convergence test for the energy of one water molecule in a cubic cell with side  $4 \text{ \AA}$  in figure 4.2. A water molecule was used since it is a small system and includes oxygen, which is the most difficult and therefore limit-setting atom.

### 4.4 Pseudopotentials

To reduce the size of the basis-set it is common to use pseudopotentials to describe the interaction between the valence electrons and the effective atomic cores with the most tightly bound core electrons. They are effective potentials which have the same properties as the true potential above a certain cutoff radius  $r_c$ , but are simpler and less computationally expensive below that radius. A nice illustration of this is shown in figure 4.3. In this work so called ultrasoft pseudopotentials [36] were used and were taken from the web page of Quantum ESPRESSO [37].

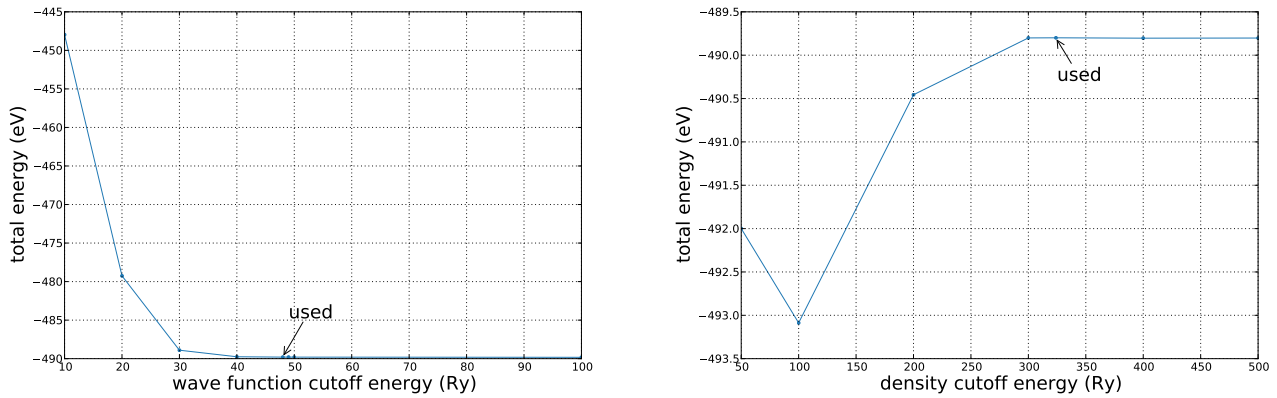


**Figure 4.2:** Convergence tests for the cutoff energies for the wave functions and the density. This is done for one water molecule in a cubic cell with side 4 Å since it is a simple system and includes oxygen, which is the most difficult and limit-setting atom.

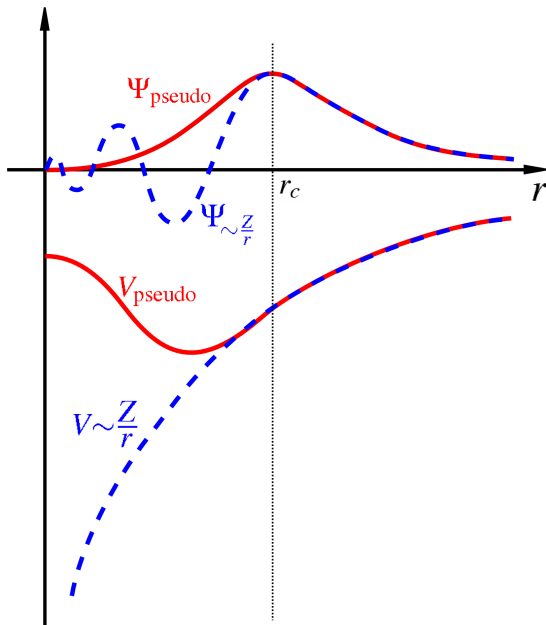


**Figure 4.3:** Comparison of a wavefunction in the Coulomb potential of the nucleus (blue) to the one in the pseudopotential (red). The real and the pseudo wavefunction and potentials match above a certain cutoff radius  $r_c$ . Note how the pseudo wavefunction has less nodes below  $r_c$  and how the pseudopotential does not diverge at zero. This makes them computationally less expensive. The figure is reprinted from Wikipedia [38].

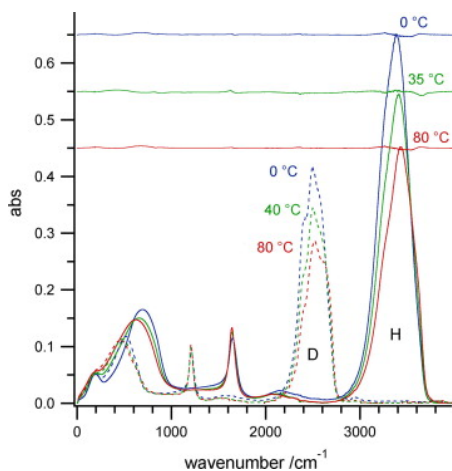


**Figure 4.4:** IR absorption spectra of water and heavy water reprinted from Maréchal 2011 [39], Copyright (2014), with permission from Elsevier.

## 4.5 Nosé-Hoover Thermostat

To control the temperature and keep it around an average in the simulation a Nosé-Hoover thermostat was used. This can be viewed as having a heat bath connected to the system which gives the particles small kicks in order to keep the system around an average temperature [19]. To do this the thermostat requires a coupling constant between the heat bath and the system. In the Quantum ESPRESSO implementation this requires the user to specify a frequency for the thermostat.

Since we do not wish to introduce extra energy into the system by hitting the atoms with a resonance frequency the Nosé-Hoover thermostat frequency should be chosen not to overlap with the eigenfrequencies of the system.

In these simulations the oscillation frequency of the Nosé-Hoover thermostat was set to 60 THz ( $2000 \text{ cm}^{-1}$ ) which is well out of the way of most peaks in the vibration spectra for water (see figure 4.4). It should be mentioned that a vibrational study of the porphyrine was never done. How the chosen frequency interact with the porphyrine is therefore not explicitly known.

## 4.6 Mean Square Displacement (MSD)

To be able to say something about the dynamics of a system it is possible to calculate the diffusion coefficient from the slope of the mean square displacement (MSD) using the Einstein relation [40, 41]

$$2tD = \frac{1}{3} \langle |\mathbf{r}(t) - \mathbf{r}(t_0)|^2 \rangle \quad (4.2)$$

where  $D$  is the self-diffusion coefficient, and  $\langle |\mathbf{r}(t) - \mathbf{r}(t_0)|^2 \rangle$  is the mean square displacement at time  $t$  compared to the positions at time  $t_0$ .

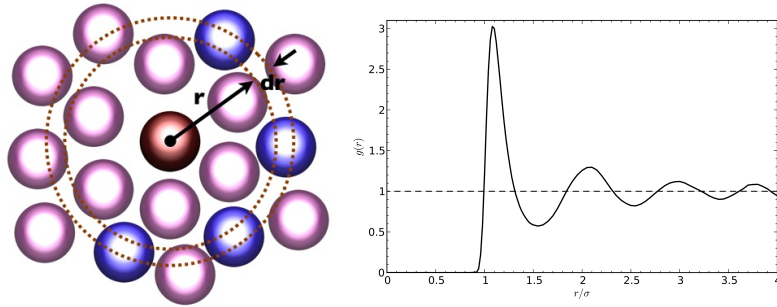


**Figure 4.5:** A schematic illustration of the radial distribution function reprinted from Wikimedia [42, 43].

For water  $\mathbf{r}(t_0)$  is the position of one oxygen atom in a water molecule at the initial time  $t_0$  and the average is over all oxygen atoms in the system.

## 4.7 Radial Distribution Function (RDF)

Another tool to analyse a system is by using the radial distribution function (RDF) or the pair correlation function. This is the average number of neighbours a particle has as a function of distance from that particle

$$g(r) = \frac{V}{N4\pi r^2 \delta r} \langle n_p(r) \rangle, \quad (4.3)$$

where  $n_p(r)$  is the number of particles at a distance between  $r$  and  $r + \delta r$  from the particle considered and  $\langle n_p(r) \rangle$  is averaged over all particles in the system. See figure 4.5.

# 5

## Results

**T**O OBTAIN A BENCHMARK for this computational setup, the reaction energies for the porphyrine and the hangman-porphyrine in vacuum were calculated. The energies were obtained by taking the structures of the different porphyrine intermediates given by Baran et al. [2] and doing a structural relaxation in order to find their ground state structure and total energy. The result for the cobalt-porphyrine is presented in figure 5.2 (top left) and is included in figure 5.3 as well. The overpotentials in vacuum in the volcano plot in figure 5.3, i.e. the distance to the equilibrium potential, is in good agreement with the previous result by Baran et al. For these calculations the simple correction for the water solvent was used as described in section 2.2.5.

### 5.1 Co-porphyrine in Water

To study the effect of the water solvent, ab-initio molecular dynamics was run for the porphyrine in water for a couple of picoseconds. The initial system was constructed by placing 45 water molecules in a random fashion in a near-ellipsoid shell with axes 10, 10 and 5 Å with a minimum O-O distance of approximately 1.9 Å. This means that the water molecules are at least 3.5 Å from the porphyrine complex.

The ab-initio molecular dynamics simulations resulted in the energy and temperature plots in figure 5.1. Demonstrated in these figures are the points which were chosen as the minimum energy configuration which was further analysed.

The structures corresponding to the chosen minimums in figure 5.1 were further analysed by running a structural relaxation with Quantum ESPRESSO's PW program. Their energies were taken as the reaction energies from DFT in equations (2.12) - (2.15). This

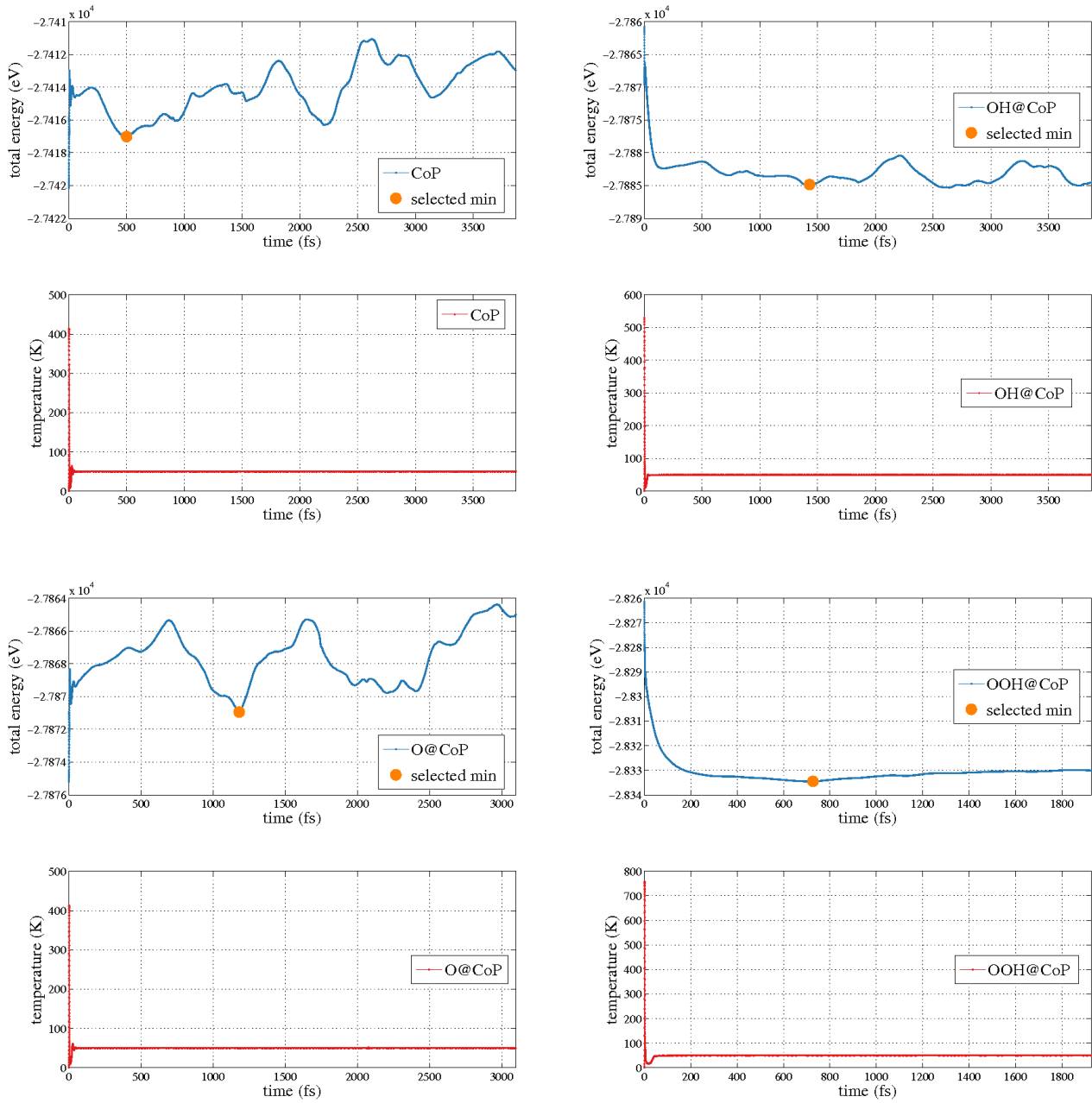


**Figure 5.1:** Energy and temperature for all porphyrine intermediates and 45 water molecules in a right-angled cell with sides 20 Å, 20 Å and 10 Å with a Nosé-Hoover thermostat with a frequency of 60 THz set around a temperature of 50 K. The simulation for the OOH intermediate is shorter than the others. This was because this system proved more difficult and more time consuming than the rest. Indicated in the energy plots are the minimum energy configurations which were selected for further study.

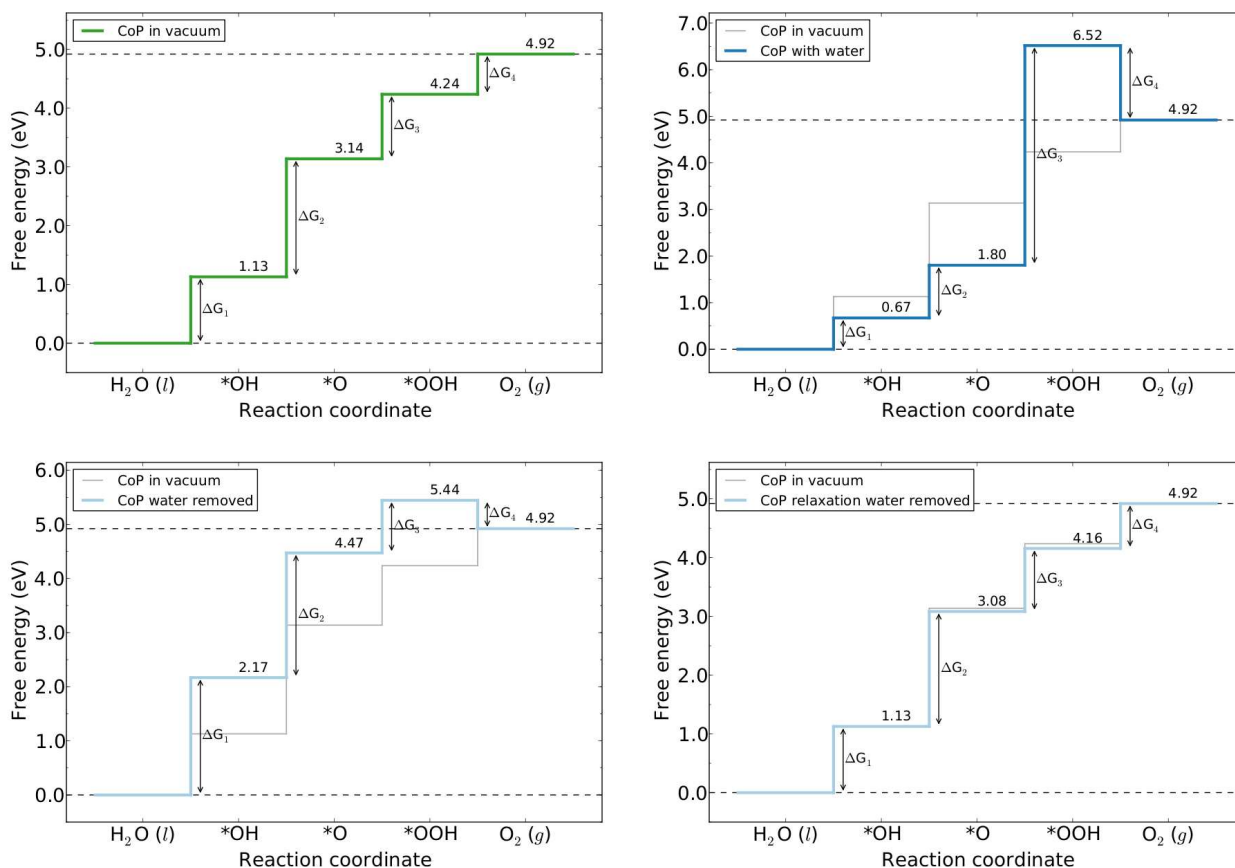


**Figure 5.2:** The reaction energies for the porphyrine in vacuum (top left), surrounded with water with structures taken from the indicated points in figure 5.1 and letting them relax (top right), when having removed the water but not relaxed the structures (bottom left) and when having removed the water and let them relax (bottom right).

resulted in the reaction steps in figure 5.2 (top right), where the steps for CoP in vacuum is plotted as a comparison. Here, no solvent correction was made since water is included. These energies are surprisingly different from the energies for the porphyrine in vacuum. This is further illustrated in figure 5.3 where the previous result by Baran et al., the results from the calculations without water and the results with water is plotted together in a volcano plot corresponding to the plot made by Baran et al. in figure 2.9. Also included are the overpotentials for the hangman-porphyrine calculated in the same way as the porphyrine without water. The important property in this figure is the distance to the equilibrium potential. Baran et al. claims that their results for the Co-porphyrine and hangman-porphyrine with the water correction are in good agreement with experimental values. The yielded results from this study in vacuum are in good agreement with these, whereas the results for the porphyrine *with* water are not.

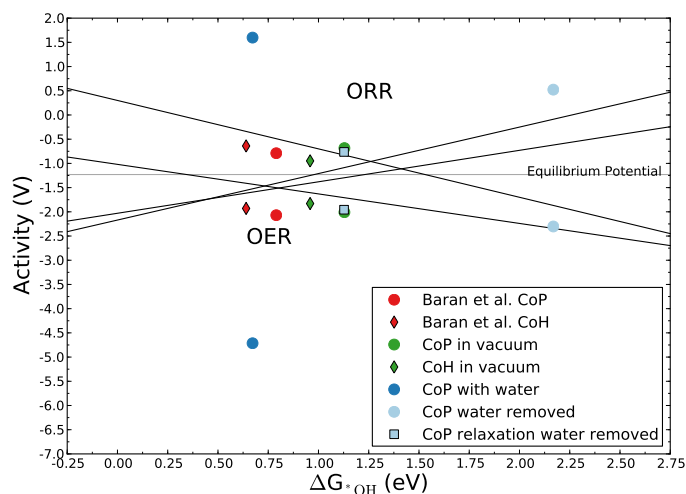


**Figure 5.3:** Volcano plot for the porphyrine and the hangman-porphyrine alone and for the porphyrine with water as well as with water removed. Note the distance to the equilibrium potential and how the results for the porphyrine with water deviates from the others.

By removing the water from the selected structures of minimum energy from the dynamics simulations and running a static PW-calculation (not doing a structural relaxation) to find the total energies, the result is closer to the vacuum case (see fig 5.2 bottom left). Since these structures were not relaxed they are not in their ground states. If these structures are relaxed to their ground states (fig 5.2 bottom right), the vacuum energies are basically retrieved. These results are also included in figure 5.3. Having removed the water, the solvent correction was used again.

**Table 5.1:** Diffusion coefficients for water simulations at different temperatures calculated from figure 5.4 according to eq. (4.2). The experimental value at 298 K is taken from [40]. The interval indicates the error of the diffusion coefficient derived from the error of the slope coefficient of the linear fits. Note how much higher than the experimental value the diffusion coefficients are.

	$T$ (K)	$D$ ( $\text{\AA}^2/\text{ps}$ )
Water	50	$1.19 \pm 0.06$
Water	200	$3.12 \pm 0.22$
Water	300	$2.63 \pm 0.13$
Expr	298	0.19
CoP	50	$1.81 \pm 0.16$
OH@CoP	50	$2.55 \pm 0.18$
O@CoP	50	$2.21 \pm 0.13$
OOH@CoP	50	$2.75 \pm 0.18$

### 5.1.1 Description of water

Why are the results with the water solvent so unlike the other reaction ladders? One attempt to try and explain this is by trying to characterize water within this setup. The following results for water are obtained by simulating only water molecules placed randomly in a uniform fashion in a cubic cell with side 9.6  $\text{\AA}$  and 32 water molecules. This is in agreement with the experimental density at room temperature [34]. The dynamics was then run in the same fashion as for the porphyrine’s reaction intermediates (described in section 4.1) at different temperatures.

One important property is the self-diffusion coefficient which can be extracted from the mean square displacement plotted against time. This is done in figure 5.4 for a water simulation to the left and for the water around the porphyrine to the right. The corresponding diffusion coefficients are tabulated in table 5.1. Note how much higher than the experimental value at room temperature the diffusion coefficients are in these simulations, regardless of temperature.

The structure of the water can be analysed by studying the radial distribution function, which is plotted for water simulated at 50 K, 200 K and 300 K in figure 5.5. Note that the result for all three temperatures are very similar. This is very much surprising since at 200 K and 50 K water should be crystalline and have distinct peaks for neighbours (and nothing in between) as in the model data from Vega et al. [44] at 220 K, while it is more like the liquid experimental data at 298 K from Soper et al. [45].

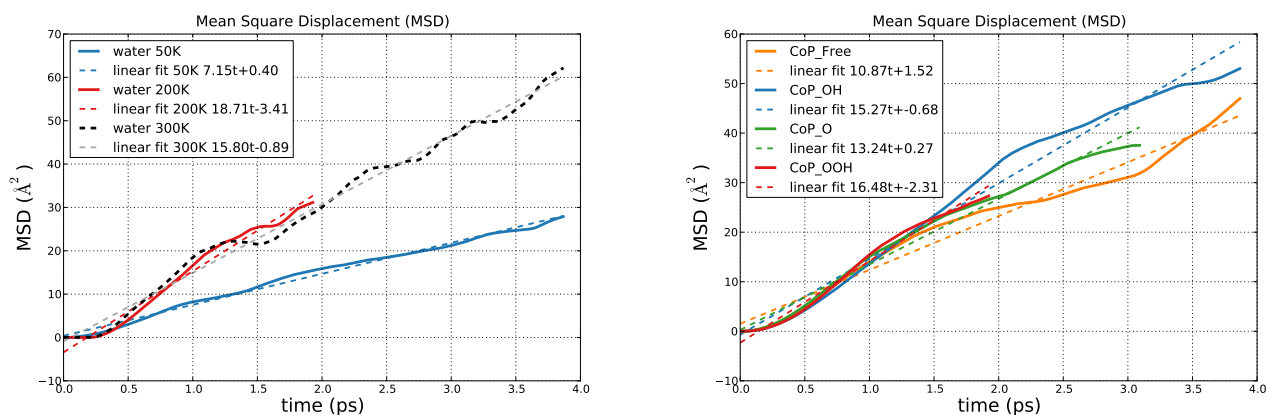


**Figure 5.4:** Mean square displacement and linear fit for an ab-initio molecular dynamics simulation of 32 water molecules in a cubic cell with side  $9.6 \text{ \AA}$  at a temperature of 50 K, 200 K and 300 K to the left. To the right: ab-initio molecular dynamics simulations of 45 water molecules and the porphyrine, the porphyrine with the \*OH intermediate, \*O intermediate and \*OOH intermediate in a right-angled cell with sides  $20 \text{ \AA}$ ,  $20 \text{ \AA}$  and  $10 \text{ \AA}$  at a temperature of 50 K. Note that the oxygens on the porphyrine are included in the MSD calculations here. Their contributions should be small.

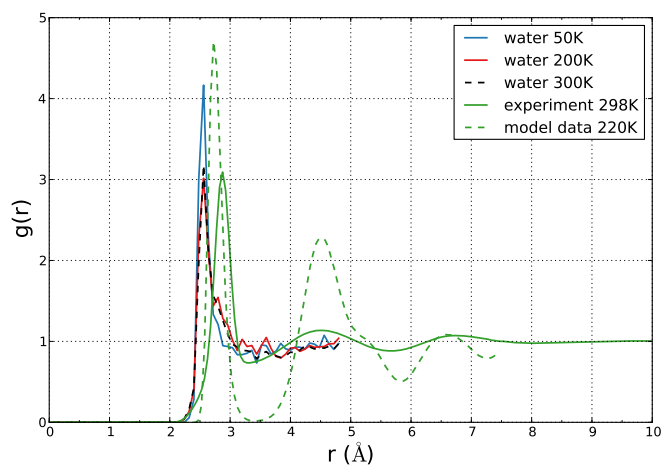


**Figure 5.5:** Radial distribution function for simulations of water at 50 K, 200 K and 300 K compared to experimental data from Soper et al. [45] and the model data for 220 K is from Vega et al. [44]. Note that water at all three temperatures have the characteristics of liquid water at room temperature (298 K).

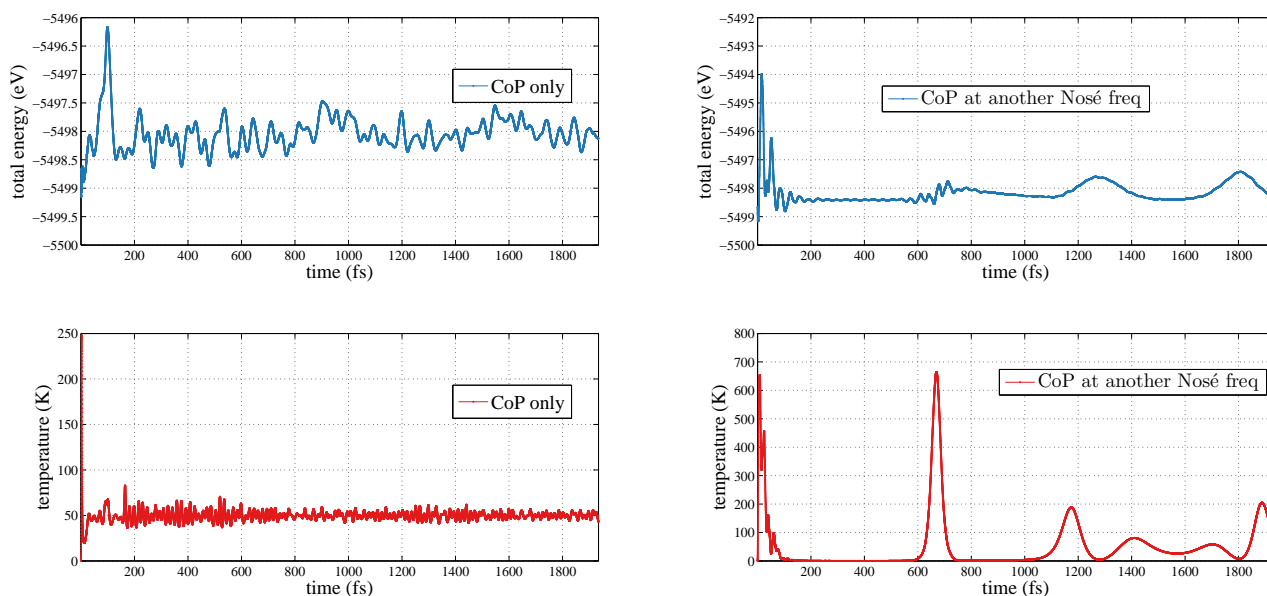


**Figure 5.6:** Energy and temperature for the porphyrine alone without water in a right-angled cell with sides 20 Å, 20 Å and 10 Å with a Nosé-Hoover thermostat with a frequency of 60 THz (left) and 3 THz (right) set around a temperature of 50 K.

### 5.1.2 Another Nosé-Hoover thermostat frequency

To further study the porphyrine, dynamics was run for the porphyrine alone as well. The energy and temperature for this simulation are presented in figure 5.6 (to the left). Also, a similar simulation was run with another Nosé-Hoover frequency (3 THz) for the thermostat (to the right). The irrational behaviour of the temperature for the frequency 3 THz, which does not oscillate smoothly around 50 K as for 60 THz, shows that this is a poorly chosen frequency which resonates quite intensely with the porphyrine. Even though a vibrational study of the porphyrine was never done, the chosen frequency of 60 THz is clearly better than 3 THz.

# 6

## Discussion

**T**HE MOST IMPORTANT property to evaluate is the overpotential of the reaction. That is how far from the equilibrium electrode potential at  $-1.23$  V the points in the volcano plot lies (figure 5.3). These are what you can hope to measure experimentally, provided there are no large activation barriers in between the steps considered here. All results will be compared to the previous result for the cobalt-porphyrine (CoP) from Baran et al. [2].

The results for the Co-porphyrine and the Co-hangman-porphyrine in vacuum agree rather well with previous results. In these calculations the correction used by Baran et al. was employed. The actual position on the x-axis is less sensitive for the presented conclusions.

### 6.1 CoP in Water

The result with water around the porphyrine is surprisingly different from the result without water. This is clearly seen in the volcano plot in figure 5.3 where the overpotential for the OER and the ORR lies very far from the equilibrium potential compared to the points for CoP in vacuum. The most important question now becomes: why are the overpotentials for the porphyrine with water included in the simulations so far from the experimentally established results?

It seems that the water in the simulations is more mobile than expected. One indication of this is in the diffusion coefficients for the oxygen atoms in these simulations as seen in figure 5.4 (to the right) and in table 5.1. These values at 50 K are much higher (about one order of magnitude) than the experimental value for water at room temperature

(298 K). Diffusion should decrease as the temperature decreases since both are a measure of movement, which is why the obtained values is claimed to be too high.

One possibility could be that the system has not reached equilibrium. This could be investigated by running the simulations for much longer, perhaps tens of picoseconds, and see if the behaviour of the system changes.

## 6.2 Water Model

The first thing one should note is that in this setup, water at 50 K does not seem to be in a solid phase. This is based on the radial distribution function and the fact that the diffusion coefficient for water at 50 K is much higher than the experimental value at 298 K. One should note that the Einstein relation (eq (4.2)) is only valid in the limit of  $t \rightarrow \infty$ , but since the energy and temperature curves have relaxed and fluctuate around an average one could argue that the system has reached equilibrium and that this approximation is okay. The errors for the diffusion coefficients were obtained by doing an error estimation of the slope of the linear fit. The intrinsic variance of the MSD values are not considered.

When taking the chosen configurations of minimum energy, removing the water and calculating the energies the result is closer to the experimental value. Letting these systems relax, the reaction energies approach those of the porphyrine in vacuum. This indicates that the problem is the water itself.

Why then is the water behaving this strangely? One possibility is that the electronic structure is very difficult and evaluated badly. If so, there could be a number of strategies to try and improve the water description. Perhaps the choice of pseudopotentials has influenced the result in an unfortunate way. Ultrasoft pseudopotentials are made to decrease the cutoff energies for the plane-wave basis set and thereby the computational cost. When there are tightly bound orbitals that have a substantial fraction of their weight inside the core region of the atom, higher cutoff energies are usually needed and one should contemplate using other types of pseudopotentials, e.g. norm-conserving potentials.

Another possibility is that the implementation in the software was not fully understood. The implementation should be tested by further studying of the different parameters on a smaller test system. It should be mentioned that the calculations with water proved more computationally expensive than initially thought<sup>1</sup>. The main obstacle for this thesis was the number of water molecules which had to be harshly reduced. It became clear that to try and study bulk water at normal density around the porphyrine would be too large a system and too time consuming. That was why these systems with one

---

<sup>1</sup>For these systems one dynamics simulation for one reaction intermediate for just below 2 ps took about 80 hours to run on 128 processors.

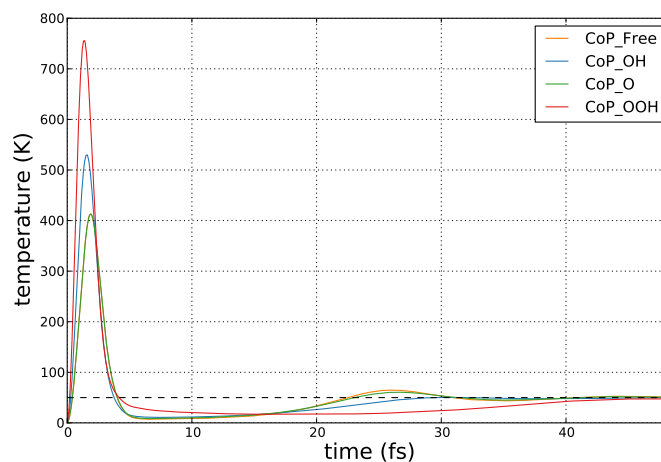


**Figure 6.1:** Temperature of the simulations of the different intermediates in the beginning. Note the rather high peak after a few fs. This is the annealing process in Car-Parrinello molecular dynamics described in section 3.5.

water shell were chosen as the initial systems. With periodic boundary conditions this effectively separates the porphyrine complexes by two mono-layers of water.

Initially the shell around the porphyrine was smaller. This caused the system to explode with motion when running the dynamics. When widening the cell in the porphyrine plane this effect was decreased. This indicates that the porphyrine is somewhat hydrophobic.

One aspect which was not studied in detail is the pressure in the system, by varying the number of water molecules in the cell with the porphyrine.

Further, the question whether the system remains on the Born-Oppenheimer surface during the simulation is unanswered. Maybe the temperature in the initial annealing (see figure 6.1) was too high and the system left the ground state. The Car-Parrinello method should work well and the system should remain on the BO surface, but there could be exceptions.

Even if a better water model was found, the model may still not accurately describe the real system of porphyrines in an electrolyte. Experimentally, the porphyrines are mixed in a solution of more than just water. Perhaps a more accurate solvent model should take that into account.

# 7

## Conclusions

**T**HE OVERPOTENTIALS FOR the OER and the ORR for the cobalt-porphyrine and cobalt-hangman-porphyrine agree well with previous work. For these calculations the simple correction for solvent effects were made.

Proceeding to the calculations for the cobalt-porphyrine including water, the results are surprisingly different. To investigate this further, the water in this implementation was further studied and found to behave in an unphysical way. This is quantified in the diffusion coefficients, which are too high compared to experimental values, and the radial distribution function, which even at 50 K has the characteristics of a liquid. When removing the water from the systems, the results approach that for the porphyrine in vacuum. From this it is concluded that the unexpected results are attributed to the water in this implementation. Continued work should try to find a better description for the water.

# Bibliography

- [1] L. Que, W. B. Tolman, Biologically inspired oxidation catalysis, *Nature* 455 (7211) (2008) 333–340.
- [2] J. D. Baran, H. Grönbeck, A. Hellman, Analysis of Porphyrines as Catalysts for Electrochemical Reduction of O<sub>2</sub> and Oxidation of H<sub>2</sub>O, *Journal of the American Chemical Society* 136 (4) (2014) 1320–1326.
- [3] J. K. Nørskov, T. Bligaard, J. Rossmeisl, C. H. Christensen, Towards the computational design of solid catalysts, *Nature chemistry* 1 (1) (2009) 37–46.
- [4] I. Chorkendorff, J. W. Niemantsverdriet, *Concepts of Modern Catalysis and Kinetics*, John Wiley & Sons, 2007.
- [5] V. Smil, Detonator of the population explosion, *Nature* 400 (6743) (1999) 415–415.
- [6] A. Hellman, K. Honkala, S. Dahl, C. Christensen, J. Nørskov, 7.17 - Ammonia Synthesis: State of the Bellwether Reaction , in: J. Reedijk, K. Poepelmeier (Eds.), *Comprehensive Inorganic Chemistry {II}* (Second Edition), second edition Edition, Elsevier, Amsterdam, 2013, pp. 459 – 474.
- [7] P. Sabatier, Hydrogénations et deshydrogénations par catalyse, *Berichte der deutschen chemischen Gesellschaft* 44 (3) (1911) 1984–2001.
- [8] Wikipedia figure: Volcano plot (May 2014).  
URL [http://en.wikipedia.org/wiki/File:Volcano\\_plot.png](http://en.wikipedia.org/wiki/File:Volcano_plot.png)
- [9] J. K. Nørskov, J. Rossmeisl, A. Logadottir, L. Lindqvist, J. R. Kitchin, T. Bligaard, H. Jónsson, Origin of the overpotential for oxygen reduction at a fuel-cell cathode, *The Journal of Physical Chemistry B* 108 (46) (2004) 17886–17892.
- [10] J. Rossmeisl, Z.-W. Qu, H. Zhu, G.-J. Kroes, J. Nørskov, Electrolysis of water on oxide surfaces, *Journal of Electroanalytical Chemistry* 607 (1–2) (2007) 83 – 89, *theoretical and Computational Electrochemistry*.

- 
- [11] F. Calle-Vallejo, M. T. Koper, First-principles computational electrochemistry: Achievements and challenges, *Electrochimica Acta* 84 (0) (2012) 3 – 11.
- [12] D. V. Schroeder, *An introduction to thermal physics*, Addison Wesley, San Francisco, 2000.
- [13] Wikimedia commons figure: Harmonic oscillator potential and wavefunctions (May 2014).  
URL [http://commons.wikimedia.org/wiki/File:Harmonic\\_oscillator\\_potential\\_and\\_wavefunctions.png](http://commons.wikimedia.org/wiki/File:Harmonic_oscillator_potential_and_wavefunctions.png)
- [14] M. T. Koper, H. A. Heering, Comparison of electrocatalysis and bioelectrocatalysis of hydrogen and oxygen redox reactions, *Fuel Cell Science: Theory, Fundamentals, and Biocatalysis* (2010) 71–110.
- [15] F. Calle-Vallejo, J. I. Martínez, J. Rossmeisl, Density functional studies of functionalized graphitic materials with late transition metals for oxygen reduction reactions, *Physical Chemistry Chemical Physics* 13 (34) (2011) 15639–15643.
- [16] D. K. Dogutan, R. McGuire Jr, D. G. Nocera, Electrocatalytic water oxidation by cobalt (III) hangman  $\beta$ -octafluoro corroles, *Journal of the American Chemical Society* 133 (24) (2011) 9178–9180.
- [17] R. McGuire Jr, D. K. Dogutan, T. S. Teets, J. Suntivich, Y. Shao-Horn, D. G. Nocera, Oxygen reduction reactivity of cobalt (II) hangman porphyrins, *Chemical Science* 1 (3) (2010) 411–414.
- [18] E. Schrödinger, Quantisierung als Eigenwertproblem, *Annalen der physik* 385 (13) (1926) 437–490.
- [19] R. M. Martin, *Electronic Structure: Basic Theory and Practical Methods*, Cambridge Univ. Press, Cambridge, 2004.
- [20] J. Thijssen, *Computational physics*, Cambridge University Press, 2007.
- [21] M. Born, R. Oppenheimer, Zur quantentheorie der molekeln, *Annalen der Physik* 389 (20) (1927) 457–484.
- [22] P. Hohenberg, W. Kohn, Inhomogeneous electron gas, *Physical review* 136 (3B) (1964) B864.
- [23] J. J. Sakurai, J. Napolitano, *Modern quantum mechanics*, 2nd Edition, Addison-Wesley, Reading, Mass., 2011.
- [24] W. Kohn, L. J. Sham, Self-consistent equations including exchange and correlation effects, *Physical Review* 140 (4A) (1965) A1133.
- [25] R. Feynman, Forces in molecules, *Physical Review* 56 (4) (1939) 340.

- 
- [26] J. P. Perdew, K. Schmidt, Jacob’s ladder of density functional approximations for the exchange–correlation energy, in: AIP Conference Proceedings, IOP INSTITUTE OF PHYSICS PUBLISHING LTD, 2001, pp. 1–20.
- [27] A. D. Becke, Perspective: Fifty years of density–functional theory in chemical physics, *The Journal of Chemical Physics* 140 (18) (2014) 18A301.
- [28] A. D. Becke, A new mixing of hartree–fock and local density–functional theories, *The Journal of Chemical Physics* 98 (2) (1993) 1372–1377.
- [29] J. P. Perdew, K. Burke, M. Ernzerhof, Generalized gradient approximation made simple, *Phys. Rev. Lett.* 77 (1996) 3865–3868.
- [30] R. Car, M. Parrinello, Unified Approach for Molecular Dynamics and Density–Functional Theory, *Phys. Rev. Lett.* 55 (1985) 2471–2474.
- [31] L. Verlet, Computer ”Experiments” on Classical Fluids. I. Thermodynamical Properties of Lennard–Jones Molecules, *Phys. Rev.* 159 (1967) 98–103.
- [32] S. Kirkpatrick, M. Vecchi, et al., Optimization by simulated annealing, *Science* 220 (4598) (1983) 671–680.
- [33] P. Giannozzi, S. Baroni, N. Bonini, M. Calandra, R. Car, C. Cavazzoni, D. Ceresoli, G. L. Chiarotti, M. Cococcioni, I. Dabo, et al., Quantum espresso: a modular and open–source software project for quantum simulations of materials, *Journal of Physics: Condensed Matter* 21 (39) (2009) 395502.
- [34] K. Laasonen, M. Sprik, M. Parrinello, R. Car, ”Ab initio” liquid water, *The Journal of Chemical Physics* 99 (11).
- [35] H. Grönbeck, I. Panas, *Ab initio* molecular dynamics calculations of H<sub>2</sub>O on BaO (001), *Phys. Rev. B* 77 (2008) 245419.
- [36] D. Vanderbilt, Soft self–consistent pseudopotentials in a generalized eigenvalue formalism, *Physical Review B* 41 (11) (1990) 7892.
- [37] Quantum ESPRESSO web page (May 2014).  
URL <http://www.quantum-espresso.org>
- [38] Wikipedia figure: Sketch pseudopotentials (May 2014).  
URL [http://en.wikipedia.org/wiki/File:Sketch\\_Pseudopotentials.png](http://en.wikipedia.org/wiki/File:Sketch_Pseudopotentials.png)
- [39] Y. Maréchal, The molecular structure of liquid water delivered by absorption spectroscopy in the whole {IR} region completed with thermodynamics data, *Journal of Molecular Structure* 1004 (1–3) (2011) 146 – 155.
- [40] I.-C. Lin, A. P. Seitsonen, I. Tavernelli, U. Rothlisberger, Structure and dynamics of liquid water from ab initio molecular dynamics—comparison of blyp, pbe, and revpbe density functionals with and without van der waals corrections, *Journal of Chemical Theory and Computation* 8 (10) (2012) 3902–3910.

- [41] J. Breed, R. Sankararamakrishnan, I. Kerr, M. Sansom, Molecular dynamics simulations of water within models of ion channels, *Biophysical Journal* 70 (4) (1996) 1643 – 1661.
- [42] Wikipedia figure: Rdf schematic (May 2014).  
URL [http://en.wikipedia.org/wiki/File:Rdf\\_schematic.jpg](http://en.wikipedia.org/wiki/File:Rdf_schematic.jpg)
- [43] Wikipedia figure: Lennard-jones radial distribution function (May 2014).  
URL [http://en.wikipedia.org/wiki/File:Lennard-Jones\\_Radial\\_Distribution\\_Function.svg](http://en.wikipedia.org/wiki/File:Lennard-Jones_Radial_Distribution_Function.svg)
- [44] C. Vega, C. McBride, E. Sanz, J. L. F. Abascal, Radial distribution functions and densities for the SPC/E, TIP4P and TIP5P models for liquid water and ices Ih, Ic, II, III, IV, V, VI, VII, VIII, IX, XI and XII, *Phys. Chem. Chem. Phys.* 7 (2005) 1450–1456.
- [45] A. Soper, M. Phillips, A new determination of the structure of water at 25 °C, *Chemical Physics* 107 (1) (1986) 47–60.